Elsevier Editorial System(tm) for Surface and Coatings Technology

Manuscript Draft

Manuscript Number:

Title: Influence of process parameters and initial microstructure on the oxidation resistance of Ti48Al2Cr2Nb coating obtained by laser metal deposition

Article Type: Full Length Article

Keywords: TiAl; coating; high-temperature; oxidation; laser metal deposition

Corresponding Author: Dr. Jenny Cecilia Zambrano Carrullo, PhD

Corresponding Author's Institution: Universitat Politècnica de València

First Author: Jenny Cecilia Zambrano Carrullo, PhD

Order of Authors: Jenny Cecilia Zambrano Carrullo, PhD; Juan C Pereira Falcon, PhD; Vicente Amigó Borrás, PhD

Abstract: Ti6Al4V have been the most important and versatile titanium alloys currently used, due to their excellent combination of low density and good mechanical properties, despite their application temperature being limited to up to 300 °C. In this work, a Ti6Al4V sheet was coated with a Ti48Al2Cr2Nb alloy by laser cladding process, with the process parameters resulting in laser-specific energy densities of 70, 80, 90 and 180 J/mm2, laser power between 600 and 900 W and scanning speed of 100 to 300 mm/min. In order to analyze the oxidation resistance at elevated temperature, isothermal oxidation tests were carried out at 800 °C for 5, 10, 25, 50, 100 and 150 hours in static air. The oxidized samples were characterized by optical microscopy (OM), scanning electron microscopy (SEM), field emission microscopy (FESEM) with energy dispersive spectroscopy (EDS), and X-ray diffraction (XRD) analysis. Two groups of coatings with similar microstructures were obtained, and their influence on the formation of thermally oxidized growth layers was studied. From the isothermal oxidation tests, it was observed that the Ti48Al2Cr2Nb coatings have good resistance to oxidation in air at 800 °C in comparison with the Ti6Al4V substrate by obtaining layers of oxides up to 12 µm thick after 150 hours of oxidation. The structure of the oxide layers is complex and comprises the growth of successive layers from the outer surface of the coating. The effect of the microstructure of the coating on the density of the oxide layer formed was evaluated.

Suggested Reviewers: Andres Gasser PhD
Researcher, Institute for Laser Technology, Fraunhofer
andres.gasser@ilt.fraunhofer.de
Specialist in laser cladding and laser metal deposition for additive manufacturing

Eli S Puchi-Cabrera PhD
Professor, UVHC, LAMIH UMR CNRS 8201, Université Lille Nord de France
eli.puchicabrera@univ-valenciennes.fr
Specialist in characterization of metallic coatings

Cleiton Carvalho Silva PhD
Professor, Engenharia Metalúrgica e de Materiais, Universidade Federal do Ceará
cleiton@metalmat.ufc.br
Specialist in high-temperature coatings and Laser Processing of metallic Materials

Mariana Mariana Staia PhD
Researcher, MSMP, Arts et Métiers ParisTech
mhstaia@gmail.com
Specialist in metallic coatings and tribology

Cover Letter

September, 17 2018
Surface & Coating Technology
Elsevier

Dear Editor, Professor A. Matthews

I am pleased to submit an original research article entitled "*Influence of process parameters and initial microstructure on the oxidation resistance of Ti48Al2Cr2Nb coating obtained by laser metal deposition*", whose authors are the Doctors: Jenny C. Zambrano Carrullo, Juan Carlos Pereira Falcon and Vicente Amigó Borrás; to be considered for publication as an original article in Surface and Coatings Technology Journal.

The article addresses the study of the influence of the initial microstructure on the oxidation behavior and resistance of TiAl coatings obtained by laser metal deposition technique with optimized parameters and using Ti48Al2Cr2Nb prealloyed powder. A wide range of specific laser energy to obtain four different coatings was used, resulting in two groups of as-built microstructures. A detailed microstructural characterization of coatings trough optical microscopy (OM), scanning electron microscopy (SEM), field emission microscopy (FESEM) with energy dispersive spectroscopy (EDS) and X-ray diffraction (XRD) analysis were used. Also a gallium focused ion beam (FIB) was used in FESEM to cut the edge of the oxidized samples to study the thickness and composition of thermally growth oxides in the cross-section. All of this to correlate the initial microstructure of the two coatings groups with the oxidation behavior through isothermal oxidation tests at high temperature. The weight gain, oxides composition and the density of the oxide layer were analyzed and correlated to the initial microstructure on TiAl laser coatings, and compared with the Ti6Al4V substrate behavior. The results confirmed that the coaxial laser cladding is a good alternative to obtain a dense TiAl coatings with high quality on Ti6Al4V, and that the TiAl laser coatings improve the oxidation behavior of this substrate evaluated at 800 °C up to 150 h.

We believe the findings on this article will be of interest of Surface and Coatings Technology Journal. We confirm that the manuscript is original, has not been published or under consideration for publication elsewhere. Further, the manuscript has been read and approved by all named authors. And the technical writing in English has been reviewed by a native speaker (and also researcher). Correspondence concerning the manuscript should be sent to the corresponding author (Jenny C. Zambrano). We hope you find our manuscript suitable for publication and look forward to hearing from you.

Sincerely,

Jenny C. Zambrano C., PhD. MSc. Eng.
Researcher
Institute of Materials Technology (ITM), Universitat Politècnica de València UPV.
Semisotano 8B. CPI, Camí de Vera s/n, 46022 Valencia. Spain.
jenzamca@upv.es
Phone: +34 660806113
Fax: +34 963877629
https://orcid.org/0000-0002-9737-7116

Highlights

We obtained dense TiAl coatings by laser metal deposition process

We studied the influence of laser parameters and initial microstructure on oxidation behavior

The as-built microstructure is of great importance in Ti48Al2Cr2Nb laser coatings

Laser metal deposition is a good alternative to thermal spray processes for high temperature coatings

Influence of process parameters and initial microstructure on the oxidation resistance of Ti48Al2Cr2Nb coating obtained by laser metal deposition

J. C. Zambrano [1 *], J. C. Pereira [2], V. Amigó [1]

[1] Instituto de Tecnología de Materiales, ITM, Universitat Politècnica de València, Camino de Vera s/n, 46022. Spain.
[2] IK4-LORTEK, Arranomendia kalea, 4A, 20240 Ordizia, Gipuzkoa, Spain.
* jenzamca@upv.es *phone: +34 651337621 fax: +34 963877629*

Abstract

Ti6Al4V have been the most important and versatile titanium alloys currently used, due to their excellent combination of low density and good mechanical properties, despite their application temperature being limited to up to 300 °C. In this work, a Ti6Al4V sheet was coated with a Ti48Al2Cr2Nb alloy by laser cladding process, with the process parameters resulting in laser-specific energy densities of 70, 80, 90 and 180 J/mm^2, laser power between 600 and 900 W and scanning speed of 100 to 300 mm/min. In order to analyze the oxidation resistance at elevated temperature, isothermal oxidation tests were carried out at 800 °C for 5, 10, 25, 50, 100 and 150 hours in static air. The oxidized samples were characterized by optical microscopy (OM), scanning electron microscopy (SEM), field emission microscopy (FESEM) with energy dispersive spectroscopy (EDS), and X-ray diffraction (XRD) analysis. Two groups of coatings with similar microstructures were obtained, and their influence on the formation of thermally oxidized growth layers was studied. From the isothermal oxidation tests, it was observed that the Ti48Al2Cr2Nb coatings have good resistance to oxidation in air at 800 °C in comparison with the Ti6Al4V substrate by obtaining layers of oxides up to 12 μm thick after 150 hours of oxidation. The structure of the oxide layers is complex and comprises the growth of successive layers from the outer surface of the coating. The effect of the microstructure of the coating on the density of the oxide layer formed was evaluated.

Keywords: TiAl; coating; high-temperature; oxidation; laser metal deposition.

1. Introduction

Titanium and its alloys are very attractive materials due to their excellent combination of properties that give them the possibility of being used in many fields of application. They are recognized for their strategic importance in the field of aeronautics as the only light metal, with very strong resistance, and are structurally effective for applications in high-performance aircraft such as jet engines and fuselage components. One of the most used alloys is Ti6Al4V, which was one of the first to be developed and is currently the most studied and used. This type of alloy has a lower weight than some low-strength steels used in the aerospace industry, as well as better corrosion resistance than some aluminum alloys, but it has low wear resistance and a limited working temperature of up to 300 °C [1–3]. Due to the need to use the Ti6Al4V alloy in high-temperature environments, and to improve its resistance to wear and oxidation, it has been proposed to coat a Ti6Al4V sheet substrate with a titanium-aluminum alloy (Ti48Al2Cr2Nb) by coaxial laser cladding process.

The laser cladding (LC) process (currently called Laser Metal Deposition, LMD) is defined by the addition of a molten material, forming a layer on the substrate surface by the overlapping of single tracks, wherein the heat source is a powerful, focused laser beam that melts the coating material (from powder or wire) and forms a metallurgical bond with the substrate. It has several advantages, including: high cooling rates, low substrate dilution, high deposition rates and low distortion [4–6].

During the last decade, considerable efforts have been made globally in the development, technology and applications of γ-TiAl-based intermetallics for long-term high-temperature operations [7]. At present, there have been advances in manufacturing technologies and a better understanding of the microstructure, deformation mechanisms, micro-alloying process and the effect of the alloying elements for these alloys [8–10].

TiAl-based alloys have been studied due to their high specific resistance at high temperatures (yield strength/density), high specific rigidity (elastic modulus/density), good fatigue resistance, creep and excellent resistance to oxidation and corrosion. The combination of these properties, along with its low density (3.7 g/cm^3), makes this alloy attractive and gives it great potential for innovative applications in advanced energy conversion systems mainly in the aeronautical and automotive industries, where these materials could replace the nickel-based superalloys that have higher densities in operation at temperatures between 600 and 800 °C. However, as a function of the microstructure, the ductility at room temperature and at high temperatures decreases due to the lack of long-range order of the intermetallics, which makes them lack fracture toughness [11–16]. Besides their poor resistance to oxidation at high temperatures, the application of Ti6Al4V alloys is limited due to the formation of unsteady and non-protective oxide layers [17,18].

In the aeronautical industry, its use is observed in components of the propulsion exhaust system, such as divergent nozzles and fins, manufactured by forging or casting, and in turbine blades in the low-pressure zone [7,19,20]. In the automotive industry, it is used in highly competitive turbochargers, specifically in turbine rotors, in vehicle engine components, including exhaust valves, replacing titanium alloys such as IMI 834 and nickel-based alloys, and in engine pistons to improve the fuel economy [7,21].

Titanium aluminides have low ductility compared to the Ti6Al4V titanium alloy, and the difference in thermal expansion of the two materials when performing the laser cladding process could generate cracks during the solidification of the coating. Therefore, heating the substrate sheet before and during the laser metal deposition process is proposed in order to minimize this effect, and because, in previous research trials, attempts to obtain coatings using this technique without sheet heating have failed. The influence of the laser beam power, nozzle scanning speed, and powder feed rate in one or several layers of TiAl coatings has

been investigated by several authors [16,22,23]; their influence on the microstructure and mechanical properties of the obtained coating is also known.

This study reports on the deposition of a TiAl-based alloy (Ti48Al2Cr2Nb) by coaxial laser metal deposition process on a Ti6Al4V substrate with different process parameters, its microstructural and phases characterization, and its oxidation behavior at 800 °C in comparison to uncoated substrate through isothermal oxidation tests.

2. Experimental procedure

Ti48Al2Cr2Nb gas-atomized pre-alloyed powder (at.%) supplied by TLS Technik (Germany) with particle size of 100-200 μm and spheroidal morphology was used, which was melted and projected onto Ti6Al4V substrate sheets (wt.%) 4 mm thick. Extensive coatings (50x50 mm^2) were obtained using a Nd:YAG solid state laser system (wavelength 1064 nm) manufactured by TRUMPF (Germany) model HL1006D with a maximum output power of 1.0 kW in continuous mode. For this study, the laser beam diameter focused on the sheet surface was 2 mm, samples were placed 8 mm from the coaxial nozzle, and the movement system consists of 4 axes table (XYZC) controlled by a Siemens digital CNC, with an overlap of 40%; the shielding gas used was helium (20 l/min). The substrate was preheated before and during the cladding process to 350 °C by a resistance heating plate below the sheet in order to prevent fissures and cracks during solidification of coating. The laser cladding process and parameters used in this study have been described by the authors in previous studies [3,23].

Four coatings with different process parameters were selected for this study (Table 1), where *S* is the scanning speed of the nozzle (mm/min), *D* is the diameter of laser beam spot, *F* is the powder feed rate (g/min), *P* is the laser beam power (W) and *E* is the specific energy, which is obtained by Equation 1.

$$E = 60\left(\frac{P}{S*D}\right) \quad \text{(Eq. 1)}$$

These selected laser coatings cover a wide specific energy range in order to study the influence of this parameter on high-temperature oxidation behavior, which will influence the initial coating microstructure.

Table 1. Laser cladding parameters. Preheat temperature of substrate: 350 ºC; overlap: 40%.

Coating	***S (mm/min)***	***F (g/min)***	***P (W)***	***E (J/mm^2)***
Coat01	300	2	700	70
Coat02	300	2	800	80
Coat03	300	2	900	90
Coat04	100	1	600	180

The cross section of the coatings was obtained by cutting, and the samples were metallographically prepared by grinding followed by polishing, and then chemically etched with Kroll's reagent. A Nikon LV100 optical microscope, a Jeol JSM6300 scanning electron microscope, and a Zeiss ULTRA55 field emission scanning electron microscope using an X-Max Oxford Instruments microanalysis system with an X-ray detector of 20 μm² installed on both SEM and FESEM were used to carry out microanalysis by energy dispersive spectroscopy (EDS) for the quantification of chemical composition. The X-ray diffraction patterns on the prealloyed powder, coating´s surface and oxidized samples were obtained using a Philips X'pert diffractometer with Cu Kα monochromatic radiation (λ= 0.15406 nm), in the range of 2θ from 20 to 90°, and analyzed using the X'Pert Plus software (PANalytical).

Samples of 8x8 mm^2 and 0.5 mm thick (TiAl clad material only) were used for the isothermal oxidation test. For this purpose, an electronic precision cutting machine was used, since it was necessary to cut only the coated portion of the substrate. Prior to cutting, the coating was rectified. In order to perform the isothermal oxidation tests at high temperatures in static air, a GALLUR muffle furnace model MC-1 was used. The test was conducted at a temperature of

800 °C and was maintained for 5, 10, 25, 50, 100 and 150 hours, with cooling in static air. Samples were weighed before and after the test using a precision weight balance, KERN brand model 770-60 with a sensitivity of 0.01 mg. An FESEM equipped with a gallium focused ion beam (FIB) was used to cut the edge of the sample and to visualize and analyze the elemental chemical composition in transverse sections of oxidized coatings through EDS microanalysis.

3. Results and discussion

3.1 Coating microstructure characterization

The laser coatings obtained show, in general, a good metallurgical bond with the substrate and a low dilution. The thickness of the coatings is in the range between 800 and 980 μm. The Figure 1 shows the cross section of the coatings Coat01 and Coat04 in the as-built condition, showing some surface cracks that have occurred during solidification and cooling, perhaps due to the difference in thermal expansion that exists between substrate and coating; minimized its quantity with the pre-heating of the substrate at 350 °C. Some small defects such as circular pores are also observed, possibly due to gas trapped during solidification, however, the defects level is lower for the coatings.

Figure 1. Cross-section of the coatings observed through optical microscopy, **a)** Coat01 coating (*E = 70 J/mm*^{2}) and **b)** Coat04 coating (*E = 180 J/mm*^{2})

Through optical microscopy, it was observed that Coat01 and Coat02 present a duplex-type microstructure formed by γ-TiAl and α_2-Ti_3Al and some areas with small amounts of α_2-Ti_3Al, specifically those close to the re-melting zones (track overlap zones) in Figures 2a and 2b.

Coat03 and Coat04 coatings have a microstructure composed mainly of grains in the light phase, identified as α_2-Ti_3Al, with a small amount of γ-TiAl dark phase lamellae in the re-melted zones (Figures 2c and 2d). The microstructure formed by γ-TiAl present lamellae in a duplex microstructure, but the one formed by the α_2-Ti_3Al phase requires higher magnifications and electron microscopy to be analyzed. The coatings can be divided into two groups, the first one formed by Coat01 and Coat02 (Low specific energy) and a second group formed by Coat03 and Coat04 (High specific energy), with similar microstructures.

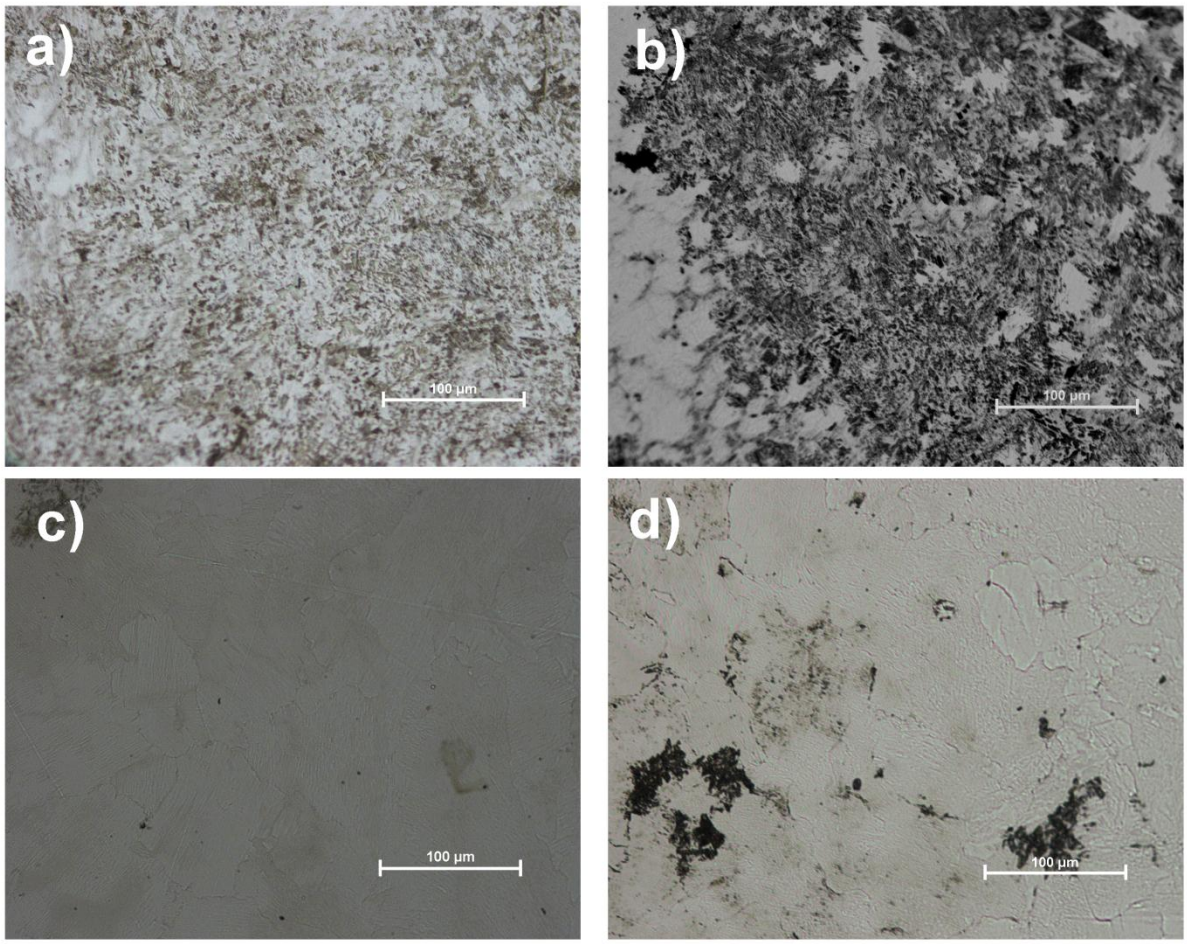

Figure 2. Coatings observed through optical microscopy, **a)** Coat01 coating (*E = 70 J/mm²*), **b)** Coat02 coating (*E = 80 J/mm²*), **c)** Coat03 coating *(E = 90 J/mm²*) and **d)** Coat04 coating (*E = 180 J/mm²*)

By using field emission scanning electron microscopy, Coat01 is observed, obtaining a thin lamellae structure (Fig. 3a), where it can be seen, based on the spectra, which the light phase corresponds to α_2-Ti_3Al and the dark phase to γ-TiAl, according to the proportion of atomic weight percentage obtained in spectrums 1 and 2, as shown in Figure 3.

The observation of the Coat04 through FESEM indicates a majority presence of α_2-Ti_3Al light phase in the entire coating, and of dark phase γ-TiAl in the re-melting areas; in Figure 3b, we have the detail of the two phases with their respective chemical composition spectra.

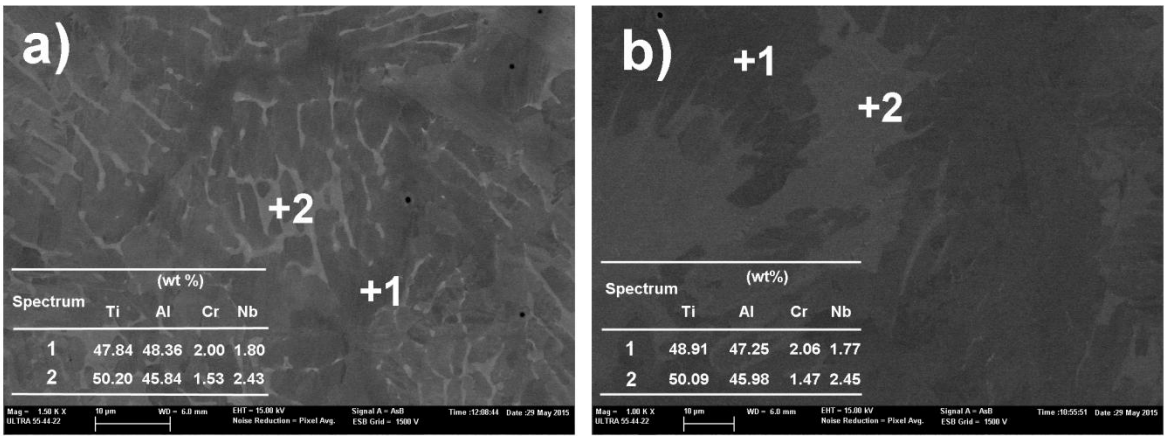

Figure 3. FESEM micrographs of initial microstructures a) Coat01 coating (Low specific energy). Detail at 1500X with spectra table, and b) Detail of Coat04 coating (High specific energy) at 1000X with spectra table

3.2 Crystallographic phases on pre-alloyed powder and coatings

Figure 4 shows the diffractograms of the Ti48Al2Cr2Nb pre-alloyed powder and corresponding laser coatings where the γ-TiAl and α_2-Ti_3Al phases can be identified, with the same proportion of the two phases being observed for the powder: for Coat01 and Coat02 coatings (70 and 80 J/mm^2), higher peak intensity corresponding to the γ-TiAl phase (dark phase in Figure 3a), and for the Coat03 and Coat04 coatings (90 and 180 J/mm^2), higher peak intensity corresponding to the α_2-Ti_3Al phase (light phase in Figure 3b), corresponding to what is observed through optical microscopy in terms of the proportion of the principal crystal phases.

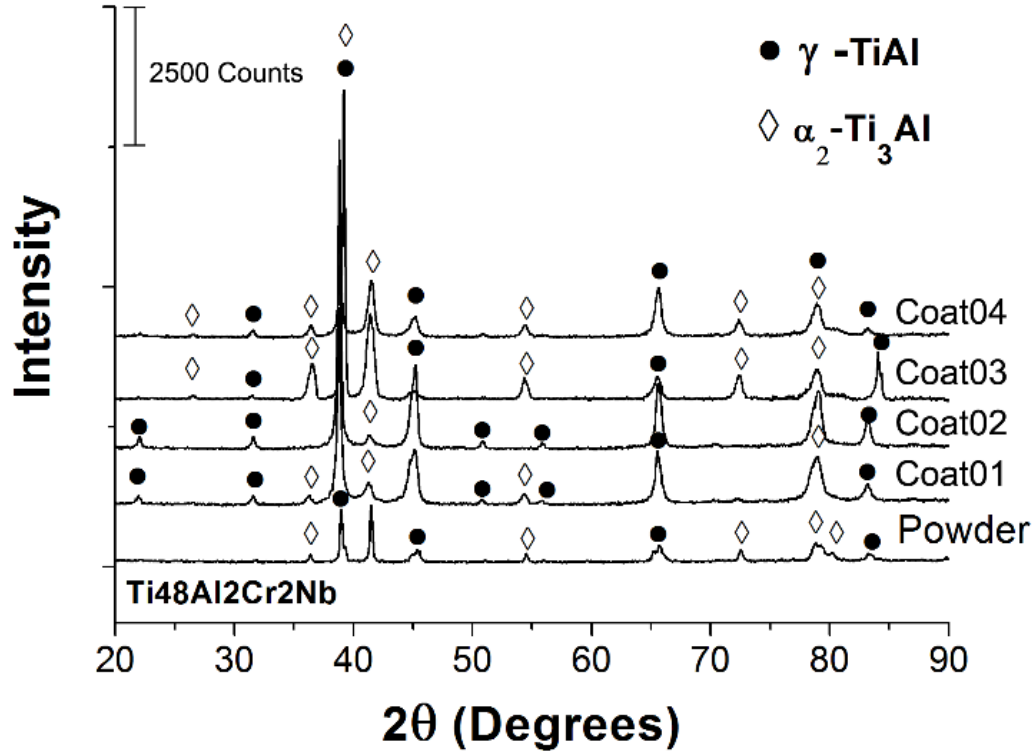

Figure 4. X-ray diffractograms of Ti48Al2Cr2Nb starting powder and coatings [3]

3.3 Oxidation resistance

The evaluation of the oxidation resistance of the substrate and the coatings was carried out in function of the weight gain obtained from the high-temperature oxidation tests and the characteristics of the formed oxide layers. The isothermal tests performed at 800 °C with furnace dwell times of 5, 10, 25, 50, 100 and 150 hours, yielded a normalized weight gain which can be observed in Figures 5a and 5b, where we can see that the Ti6Al4V substrate has a normalized weight gain ten times greater than the Ti48Al2Cr2Nb coatings. Figure 5b shows only the weight gain of the coatings; we can observe differences between them. It can be noted that they are divided into two groups, a first group formed by Coat01 and Coat02 (Low specific energy) presenting a lower weight gain, and a second group formed by Coat03 and Coat04 (High specific energy) with greater weight gain, with these groups differing in their microstructure as described above.

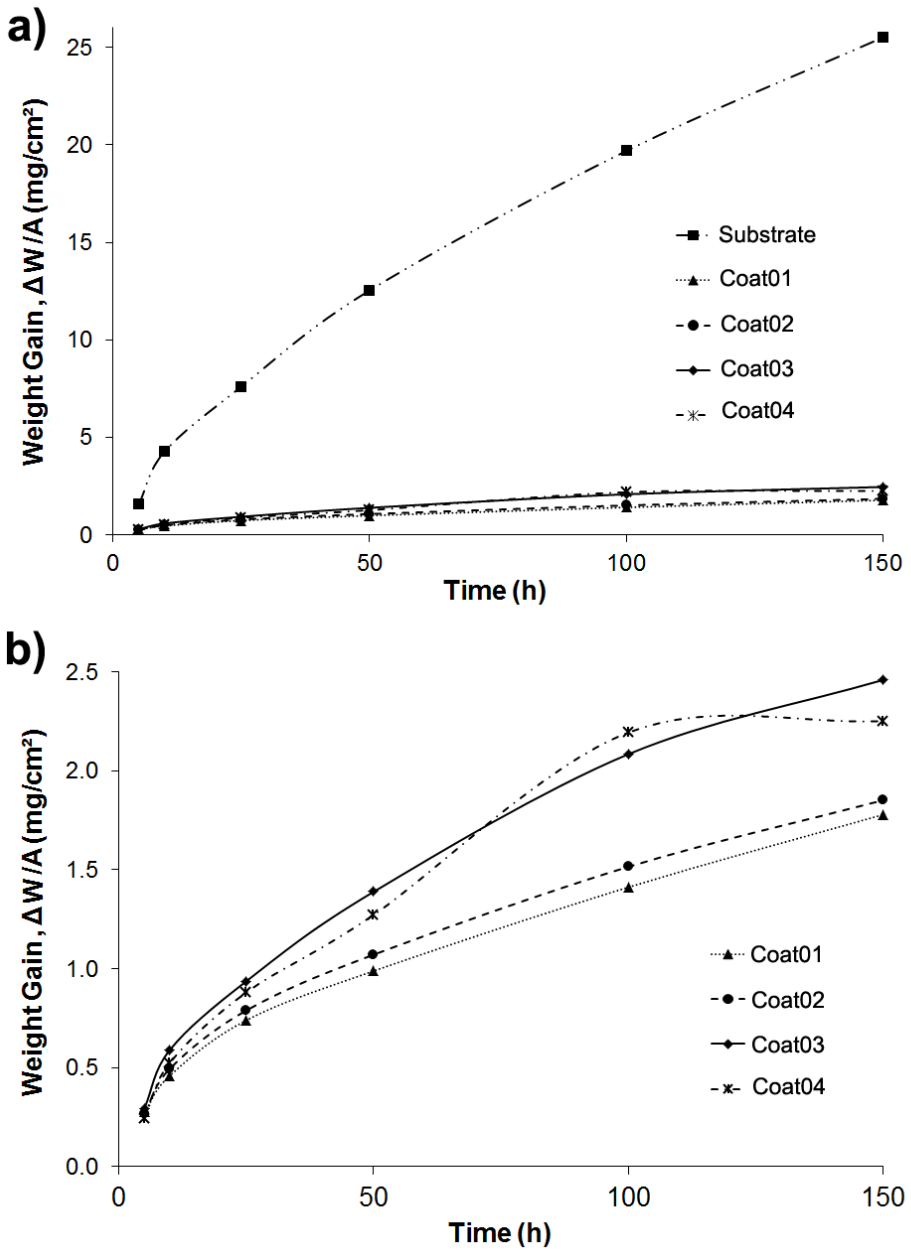

Figure 5. Normalized weight gain as a function of oxidation time for isothermal tests, **a)** Substrate and coatings, **b)** Coatings Coat01 and Coat02 (Low specific energy), Coat03 and Coat04 (High specific energy), where it can be seen that they are separated into two groups according to their behavior

The oxidation weight gain of the Ti6Al4V substrate reported by *Jeng et al.* [24] is similar in orders of magnitude to that obtained in this study. This normalized weight gain of the substrate presents oxidation kinetics that have been approximated with a mathematical model to an increasing potential curve, following the equation: $\Delta W/A = 0.0058\ t^{0.7734}$, where ΔW represents the weight gain (mg), A is the total area of the exposed surface (cm^2) and t is the oxidation time (h).

Normalized weight gain as a function of oxidation time of the coatings can be represented in two stages: a first section with increasing potential behavior up to 50 hours of oxidation, and then a second section with linear behavior as a function of time (Figure 6) from 50 to 150 hours. These are shown with dashed lines for one coating of group 1 (Coat01: Low specific energy) and for one coating of group 2 (Rec3: High specific energy).

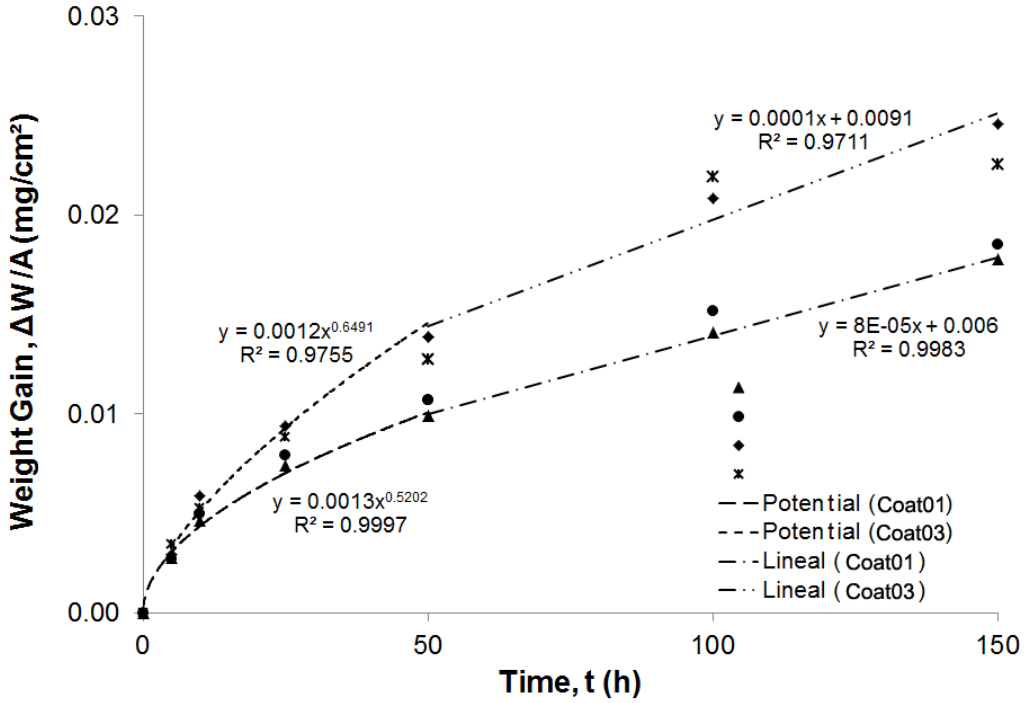

Figure 6. Normalized weight gain curves with respect to test time at 800 °C, which include the equations of the curves for Coat01 and Coat03 (Low and High specific energy)

The Coat01 coating obtained up to 50 hours has a lower weight gain; the adjusted equation for this coating has a smaller exponent in the potential equation of weight gain than that obtained for Coat03, indicating a more stable growth of the oxide layer as a function of oxidation time, denoting a lower oxidation rate up to 50 h. As for the linear behavior of the oxide layer growth after 50 hours, Coat01 presents a smaller slope of the line with respect to Coat03, which indicates a lower growth rate of the oxides layers, and is associated with the scant variation in the size of the oxide crystals observed on the surface.

The coatings in group 2 (Coat03 and Coat04: High laser specific energy) gained 35.6% more weight during 150 h oxidation than group 1 (Coat01 and Coat02: Low specific energy). The

fitted equations for the coatings in the two stages and their adjustment factor (or correlation coefficient, R^2) are compiled in Table 2, where it can be seen that they present lower oxidation kinetics than those found for the Ti6Al4V substrate, as seen through the multiplier coefficient and exponent of their weight gain equation.

The observed weight gain for the obtained laser coatings indicates that there is diffusion of titanium and aluminum in a process considered as potential growth kinetics in the initial stages of the oxidation process, with normalized weight gain values similar to obtained at 800 ºC a casting Ti48Al2Cr2Nb alloy [25]. In order to be able to consider that the formation of a stable oxide layer exists, we must have a flat region in the curve over the time, but this is not observed in the linear stretch of the weight gain behavior (Figure 6); at least, not within the 150 hours of the isothermal test that were conducted in this work.

Table 2. Equations of potential and linear weight gain behavior, as a function of oxidation time in two TiAl laser cladding coatings

Coating	***Range***	***Weight gain equation (t in h and ΔW/A in mg/cm^2)***	***Correlation coefficient, R^2***
Coat01	0-50 h	$\Delta W/A = 0.0013\ t^{0.5202}$	0.9997
	50-150 h	$\Delta W/A = 0.00008\ t + 0.006$	0.9983
Coat03	0-50 h	$\Delta W/A = 0.0012\ t^{0.6491}$	0.9755
	50-150 h	$\Delta W/A = 0.0001\ t + 0.0091$	0.9711

3.4 Characterization of oxides obtained in isothermal tests

The surfaces of the oxidized samples were observed by scanning electron microscopy (SEM) in order to obtain the crystal size and analyze the morphology of the surface oxide crystals formed during the isothermal tests; the images obtained at similar magnification are shown for comparison purposes in Figures 7 to 9 below.

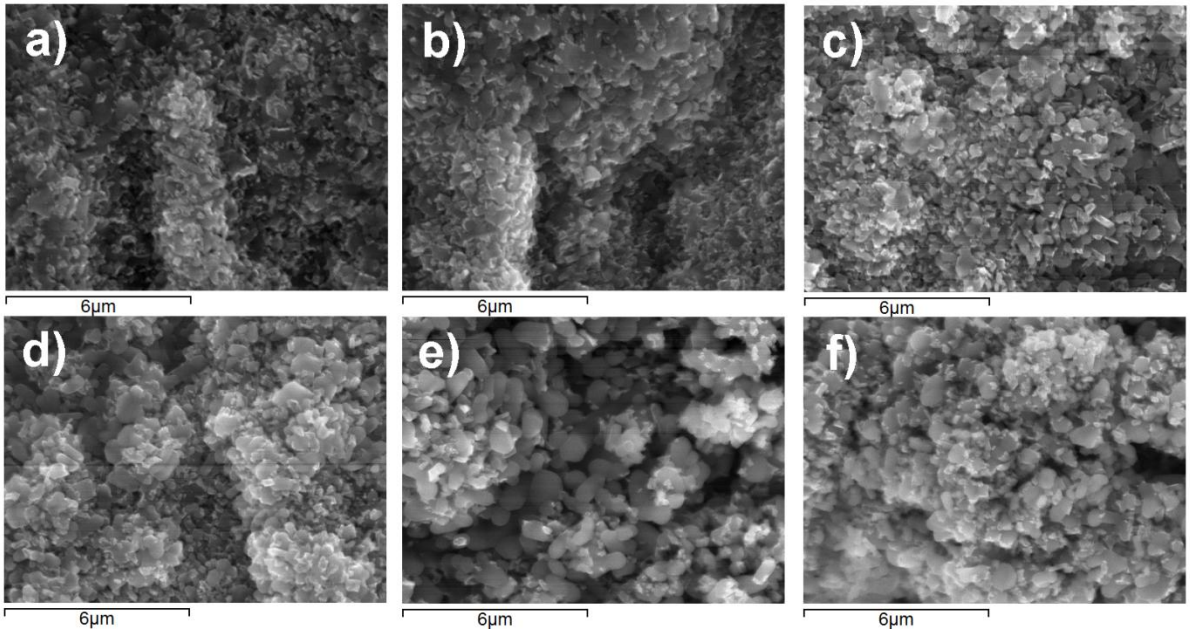

Figure 7. SEM micrographs, oxide morphologies of substrate Ti6Al4V oxidized at 800 ºC, **a)** 5 hours, **b)** 10 hours, **c)** 25 hours, **d)** 50 hours, **e)** 100 hours, and **f)** 150 hours

A layer of TiO_2 and Al_2O_3, in the form of agglomerates with a size range of 0.25 µm to almost 1 µm, grew on the oxidized substrate samples. The agglomerates are very small, and after 5 hours (Figure 7a), they cover the entire substrate surface, increasing in size with exposure time in the furnace (Figure 7b to 7f).

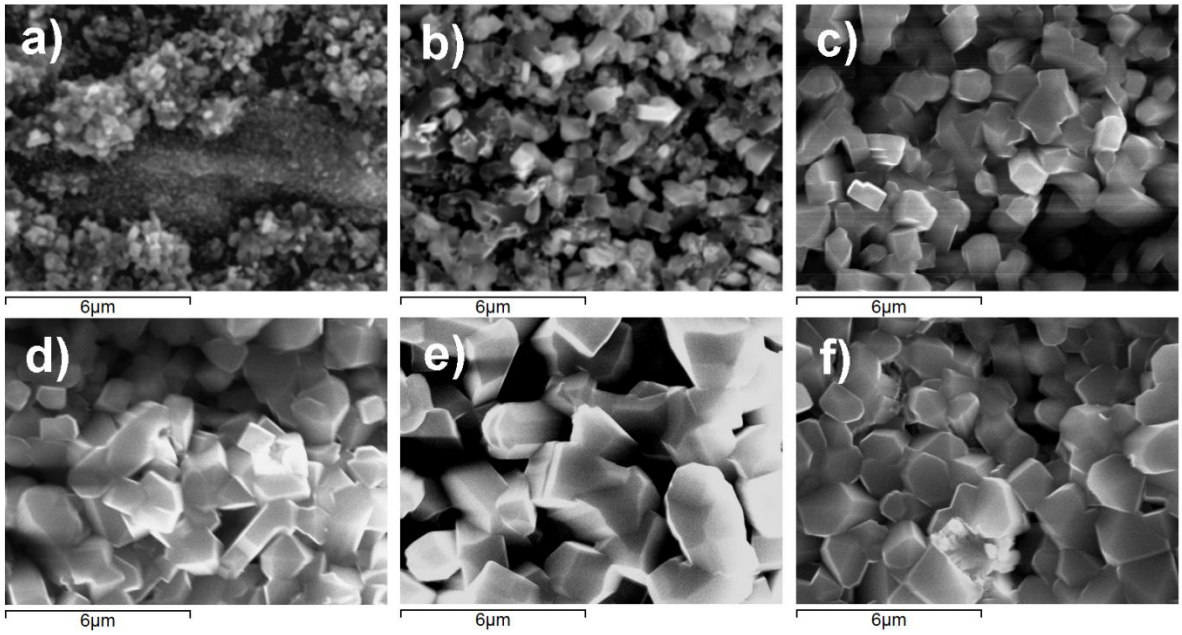

Figure 8. SEM micrographs, oxide morphologies of Coat01 coating (Low specific energy), **a)** 5 hours, **b)** 10 hours, **c)** 25 hours, **d)** 50 hours, **e)** 100 hours, and **f)** 150 hours

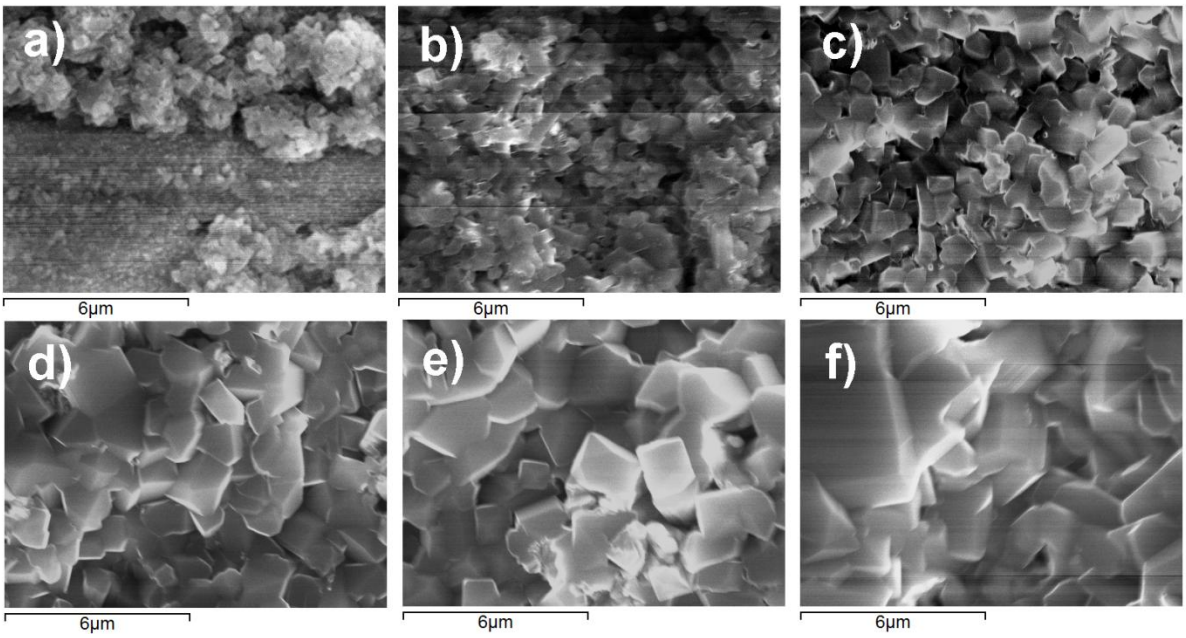

Figure 9. SEM micrographs, oxide morphologies of Coat04 coating (High specific energy), **a)** 5 hours, **b)** 10 hours, **c)** 25 hours, **d)** 50 hours, **e)** 100 hours, and **f)** 150 hours

The formation of oxide layers on the surface in the form of agglomerates of about 0.25 µm can be observed in Figure 8a for coating Coat01, at 5 hours, where the coating is not yet fully covered (some areas without crystals). These oxides increase in size and cover all coating´s surface with increasing exposure time at 800 °C, and then grow in the form of pillars which intersect, giving rise to a porous layer of TiO_2, with oxides of an average size of 2 µm for 100 h (Figure 8e). On the Coat04 coating (Figure 9), 5-hour agglomerates of very small oxides are observed, increasing in size up to about 4 µm for 150h (Figure 9f). In order to obtain a clearer view of the surface oxides, techniques such as X-ray diffraction pattern have been used to identify the crystal phases present in the oxidized surface of Coat01 (Figure 10a) and Coat04 (Figure 10b) coatings, as shown in the diffraction patterns presented.

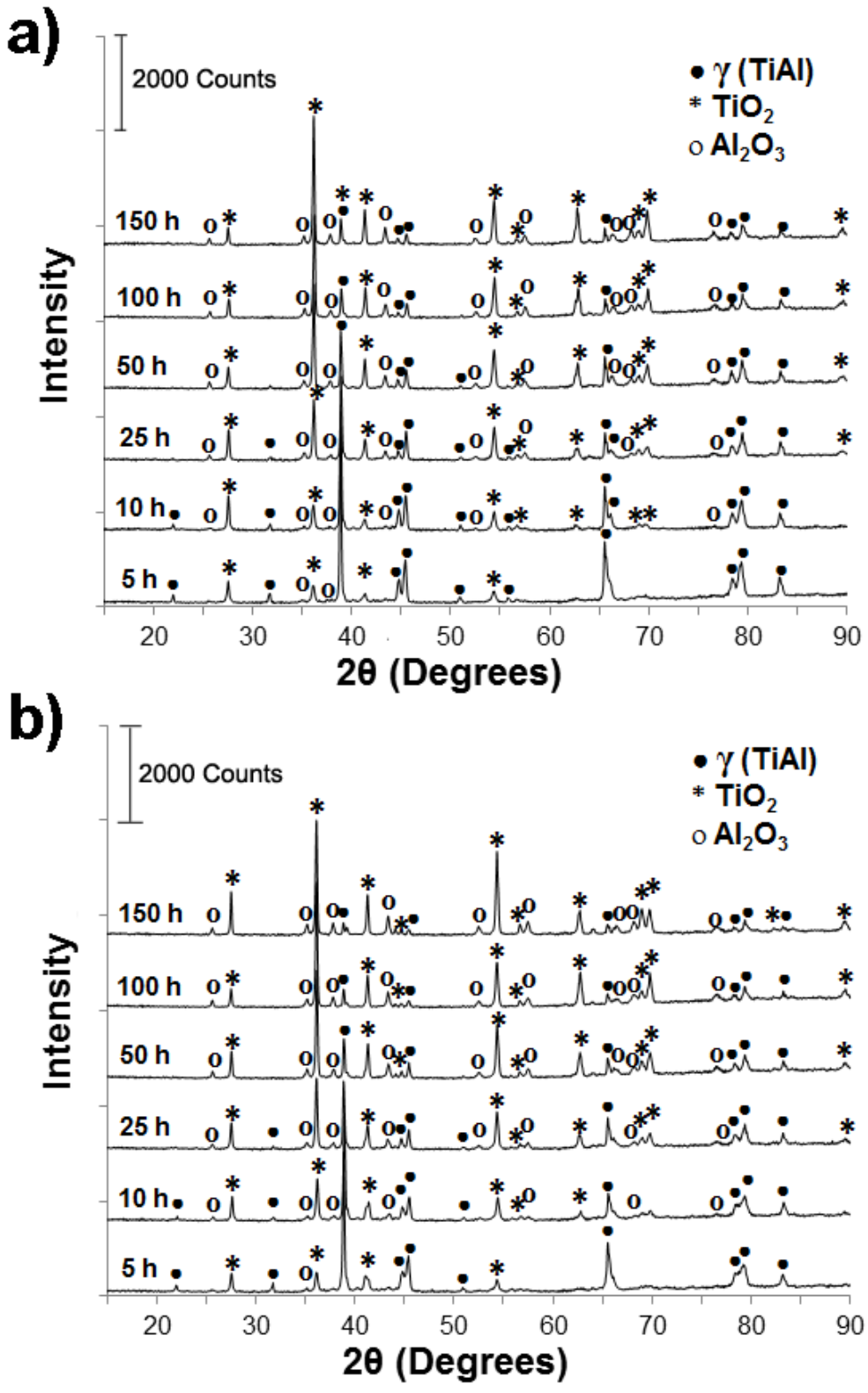

Figure 10. X-ray diffractograms of the coatings: **a)** Coat01 and **b)** Coat04, both tested isothermally at 800 °C for 5, 10, 25, 50, 100 and 150 hours

For the two coatings, Coat01 and Coat04, peaks correspond to the γ-TiAl phase of the coating, in addition to the presence of the oxides TiO_2 and Al_2O_3, for 5 and 10 hours. After 25

hours, a few main peaks of the coating disappear, and it is observed that the peaks corresponding to the alumina have low intensity but remain constant until 150 hours; in the case of TiO_2, there is an increase in the intensity of some peaks by increasing the oxidation time at 800 °C. The phases in the diffractograms correspond to those in the oxidized surfaces of the coatings observed in Figures 8 and 9, where, at 5 and 10 hours, the coating is still observed due to the low thickness of the oxide film. From there, a mixture of the two types of oxides is observed in agreement with the diffractograms.

In Figures 8 and 9, it is observed that the oxides initially appear as agglomerates and grow over time up to 25 hours, and then present a pillar growth with a relatively constant crystal size with increasing furnace time at 800 °C. For all cases, it is observed that the surface layer of oxides is porous due to the lateral growth of the oxides, which is in agreement with other authors and the expected behavior for the TiO_2layer, which is the external layer obtained in this process of isothermal oxidation [25–29]. It is very important to note that the oxides grow rapidly up to 25 hours, corresponding to the potential weight gain behavior, and then continue to increase in a linear and stable fashion but with no apparent growth of size in surface oxide crystals.

Although the diffusivity of oxygen ($4x10^{-19}$ m^2/s 900 °C) in TiAl is five orders of magnitude lower than titanium, which makes it more resistant to corrosion than some Ti alloys, it is a critical factor for γ-TiAl structures at temperatures above 800 °C for long exposure times, especially under cyclic thermal conditions [30]. The improvement in corrosion resistance is based on the elements that constitute and are added to these alloys, which are selectively oxidized and will produce a protective layer of oxide at the surface.

For Ti-Al binary alloys, the oxidation products are mainly rutile (TiO_2) and alpha alumina (α-Al_2O_3), as has already been observed in this investigation with laser cladding processing and fast cooling rate. By comparison with alumina, rutile has greater diffusivity and offers poor

protection; however, both can be formed simultaneously. The formation of a continuous layer of alumina is a prerequisite for achieving sufficient oxidation resistance. TiAl alloys such as the one used in our laser coatings do not have a sufficient percentage of aluminum to form this layer, since it is known that with 50% or less of Al, rutile will form instead of alumina as a stable phase; other studies have shown that 60 to 70% Al is required to form a stable layer of alumina in air, and 47-48% in oxygen [30].

3.5 Cross section of thermally grown oxides

A cross section analysis of the oxide layer was used to observe its constitution and evolution. These observations are made in two coatings, Coat01 and Coat04, because they present different initial microstructures and because they have different weight gain, as reported above. Three intermediate oxidation times: 10, 25 and 100 hours were used, since at 5 h the surface has not yet been covered with oxide, and at 150 hours a negligible difference is observed compared to 100 hours. This observation aims to measure the thickness of the total oxide layer and observe its homogeneity, as well as to differentiate the different layers of oxides present.

The cross sections of oxidized coatings are shown in Figure 11, where an increase in the thickness of the oxide layer is observed by increasing the exposure time in the furnace during the isothermal oxidation test. It is observed that there are several layers of oxides, light gray or dark gray when observed by field emission electron microscopy, where the outermost layer is porous and the intermediate layers are homogeneous. The FESEM observations of the layers formed, with their respective EDS microanalysis, were used.

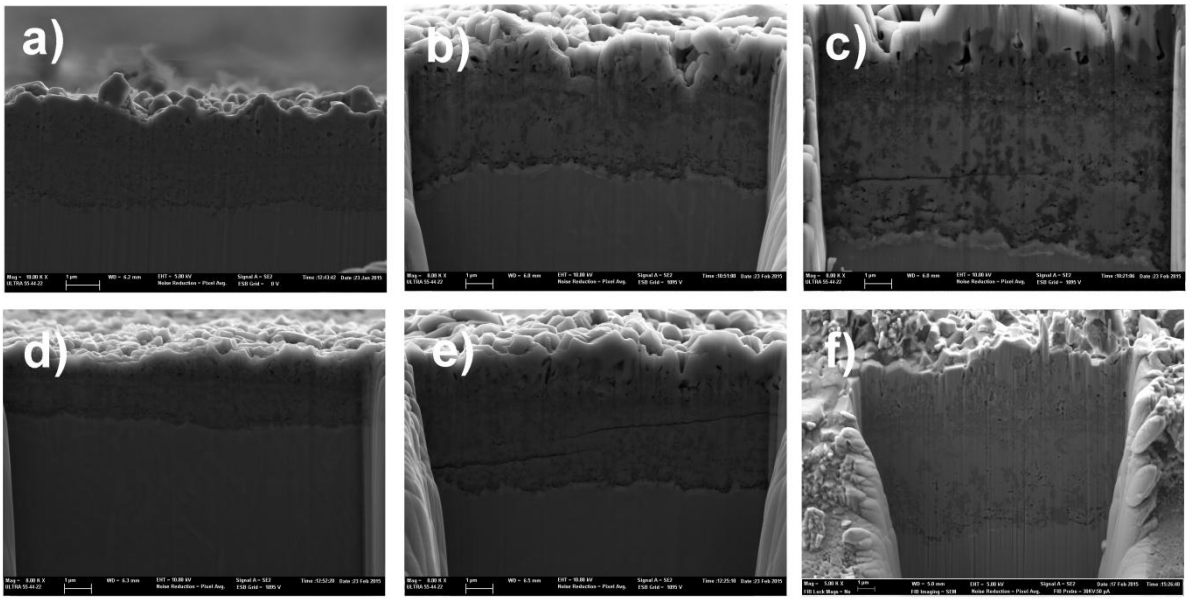

Figure 11. Cross section of the oxide layer observed by field emission electron microscopy (FESEM). Coating Coat01 (Low specific energy) with different test times: **a)** 10 hours, **b)** 25 hours, **c)** 100 hours; Coat04 coating (High specific energy): **d)** 10 hours, **e)** 25 hours, and **f)** 100 hours

Figures 12 to 15 depict the transverse section of the oxide layers for the Coat01 and Coat04 coatings tested at 800 °C for 10 hours and 25 hours, EDS analysis by line scanning in coatings, the chemical composition of the layers, as well as an increase in the thickness of the intermediate layer as the oxidation time increases. In the case of Coat04, spectra of the detail of the oxide/coating interface are presented.

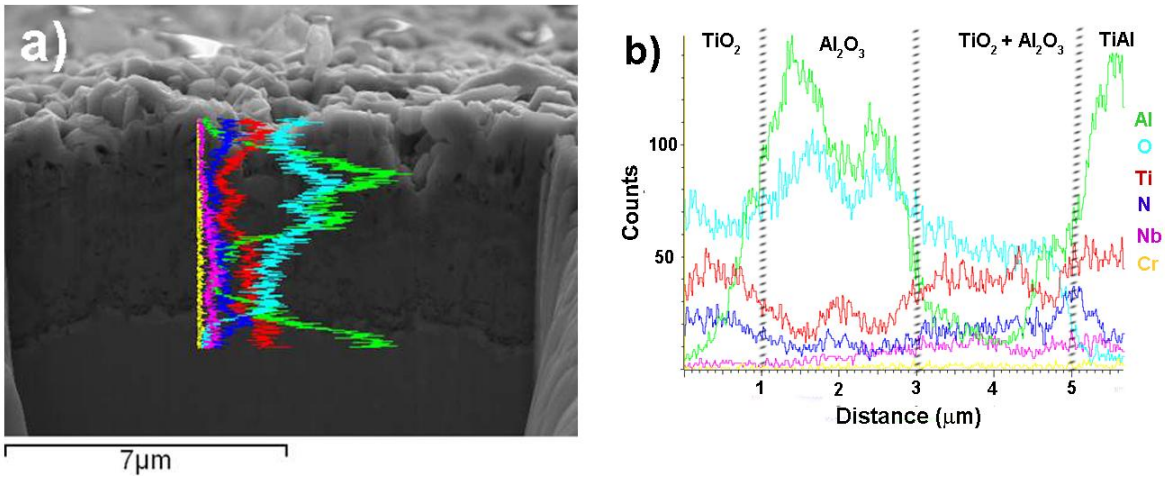

Figure 12. Coat01 (Low specific energy) oxidized coating up to 25 hours, **a)** SEM micrograph of cross section and **b)** EDS microanalysis line scan

During the initial stage of isothermal oxidation, a mixture of α-Al_2O_3, TiO_2, Ti_2AlN and TiN is formed, as can be seen in the cross-sectional figures, where the light phase corresponds to TiO_2, the dark phase corresponds to Al_2O_3, and a nitrogen-rich zone is obtained at the interface, as reported by *Varlese et al.* [29].

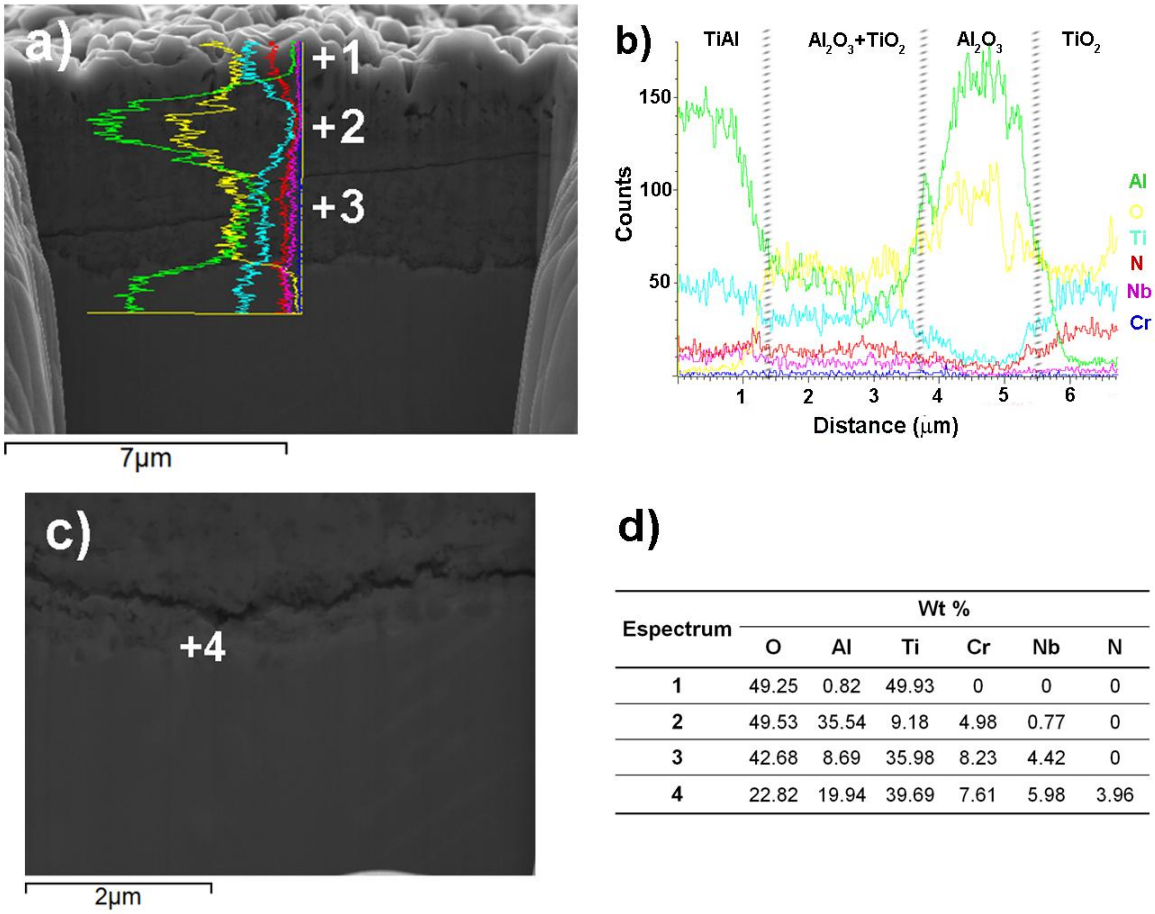

d)

Espectrum	Wt %					
	O	Al	Ti	Cr	Nb	N
1	49.25	0.82	49.93	0	0	0
2	49.53	35.54	9.18	4.98	0.77	0
3	42.68	8.69	35.98	8.23	4.42	0
4	22.82	19.94	39.69	7.61	5.98	3.96

Figure 13. Oxide layers of Coat04 coating (High specific energy) tested at 800 °C for 25 hours. **a)** Transverse section of the layer, **b)** Linear analysis by EDS, **c)** Detail of metal-oxide interface zone, and **d)** Table results of EDS spectrums in Figures 13a and 13c

It was observed the α-Al_2O_3 + TiO_2 layer grows rapidly after a long exposure time. A low oxidation rate during the initial state can be explained by the formation of a relatively dense and protective oxide layer, with an outer layer rich in alumina, which may act as a barrier layer, since the alumina may be slightly more stable than TiO_2 and there is no preferential oxidation if the two metals have the same activity.

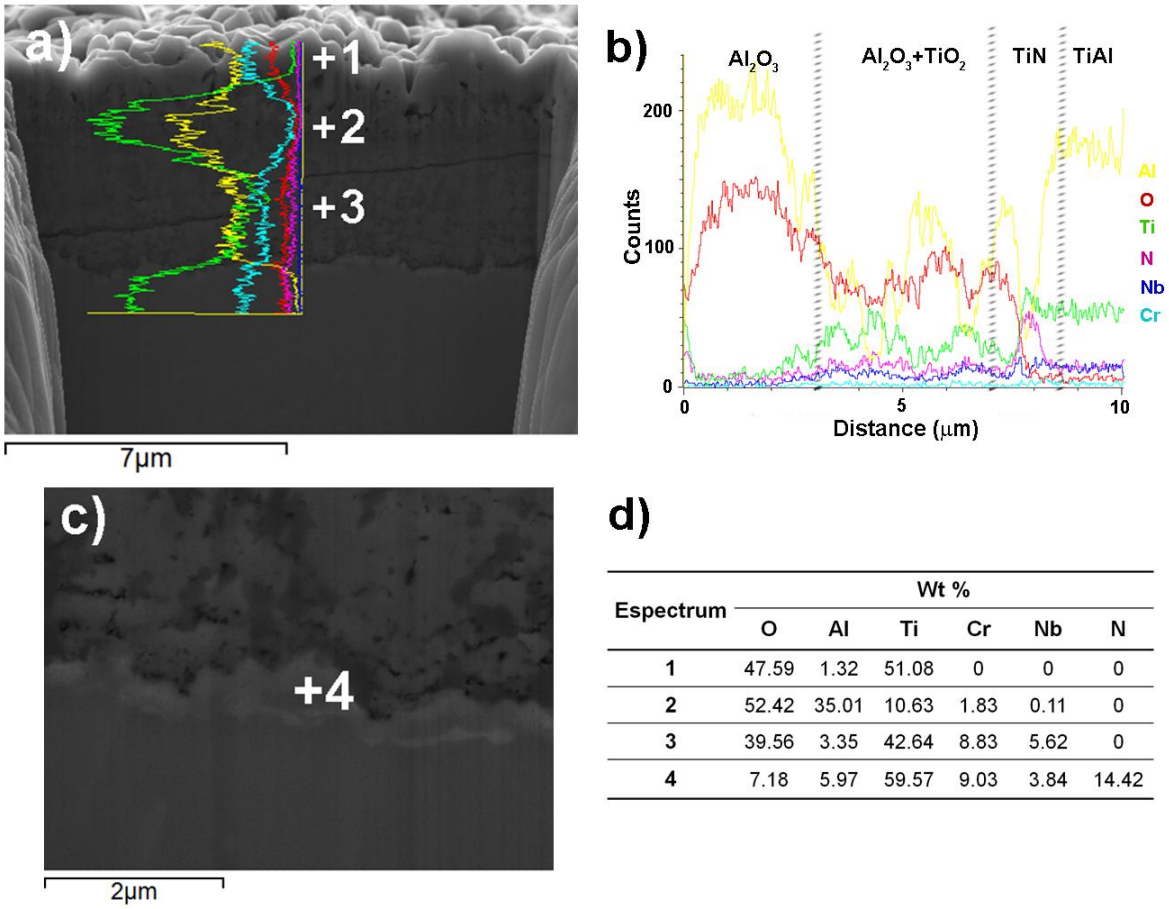

d)

Espectrum	Wt %					
	O	Al	Ti	Cr	Nb	N
1	47.59	1.32	51.08	0	0	0
2	52.42	35.01	10.63	1.83	0.11	0
3	39.56	3.35	42.64	8.83	5.62	0
4	7.18	5.97	59.57	9.03	3.84	14.42

Figure 14. Oxide layers of Coat01 coating (Low specific energy) tested at 800 °C for 100 hours. **a)** Transverse section of the layer, **b)** Linear analysis by ESD, **c)** Detail of metal-oxide interface zone, and **d)** Table results of chemical composition in indicated spectrums

For the Coat01 tested at 100 h, the same layers are formed as at 10 and 25 hours, but with greater thickness. In this case, the presence of a high nitrogen content in the interface is observed, as detailed in Spectrum 4 of Figure 14, in agreement with the spectra of the rest of the layers. Figure 15 shows the cross section of the oxide layers obtained for Coat04 tested for 100 hours, where the presence of the different layers is verified, and it is observed that the intermediate mixture layer increases its thickness after the oxidation time has elapsed.

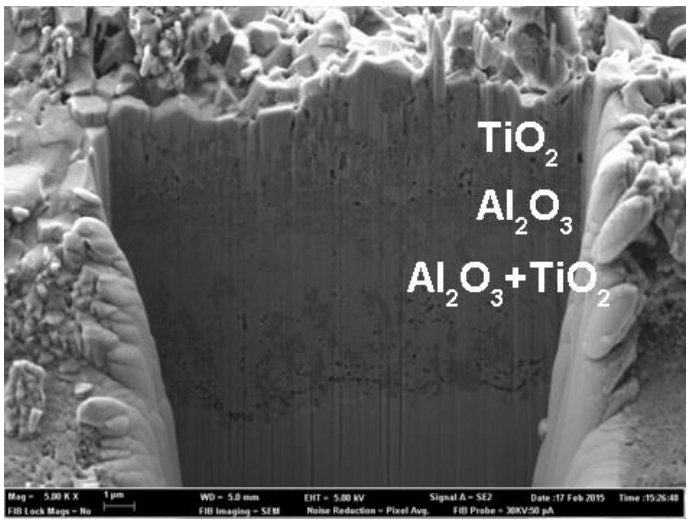

Figure 15. Oxides layers in Coat04 coating (High specific energy). Sample tested at 800 °C for 100 hours

After a transition period, the oxidation rate increases; in this case, it has been verified that this is from 50 hours according to the weight gain curves, and increases the porous outermost layer of mainly TiO_2. In this layer, a thickening of particles is present, and the thickness increases over time. The formation of the pores underneath and within the layer can been explained by the initial growth of the crystals, almost perpendicular to the surface, followed by lateral growth until they meet with each other. The formation of this outer layer of TiO_2 can be explained by the outward diffusion of titanium through the discontinuous alumina layer. Some authors such as *Haanappel et al.* [26] and *Becker et al.* [31] suggest that the alumina layer is permeable for both Ti and O_2 ions; this layer is observed for all cases of oxide layers in the coatings just below the rutile, with the exponent observed in the adjustment of the weight gain curve. The continuous growth of the inner oxide layer, composed of a mixture of α-Al_2O_3 + TiO_2 below the outer layer of alumina, can be explained by the diffusion of oxygen into the interior, possibly along intergranular zones.

The growth of the TiO_2 layer after long exposure times on the outer surface of the laser coatings can be explained by the outward diffusion of the titanium ions. Inward diffusion of oxygen was confirmed by two-state oxidation experiments [26]. It can be clearly observed that the oxide growth occurs at the oxide/gas interface where a significant oxygen transport is

observed in the interior. Due to the simultaneous diffusion of the oxygen into the interior and of the titanium towards the outside, the TiO_2 can precipitate through channels, which act as paths for the titanium from the inner zone of the oxide towards the outer zone of the TiO_2 layer. Due to this, the alumina loses its protective condition and is divided into islands in a porous layer of TiO_2, which is explained by the TiO_2 having significant solubility in the alumina [26].

It is indicated that a greater thickness of oxide layers is related to more permeable layers. As the layer is less stable, it continues to grow without reaching the stability that would provide a protective layer. It is expected that the oxidation resistance will be lower, as has been seen; weight gain in the coatings follows a growing and then linear potential, which corroborates this behavior. As can be seen in Figure 15, the Coat04 coating with higher specific energy has a higher oxide layer thickness than Coat01 (Low specific energy), which is explained by its different microstructure.

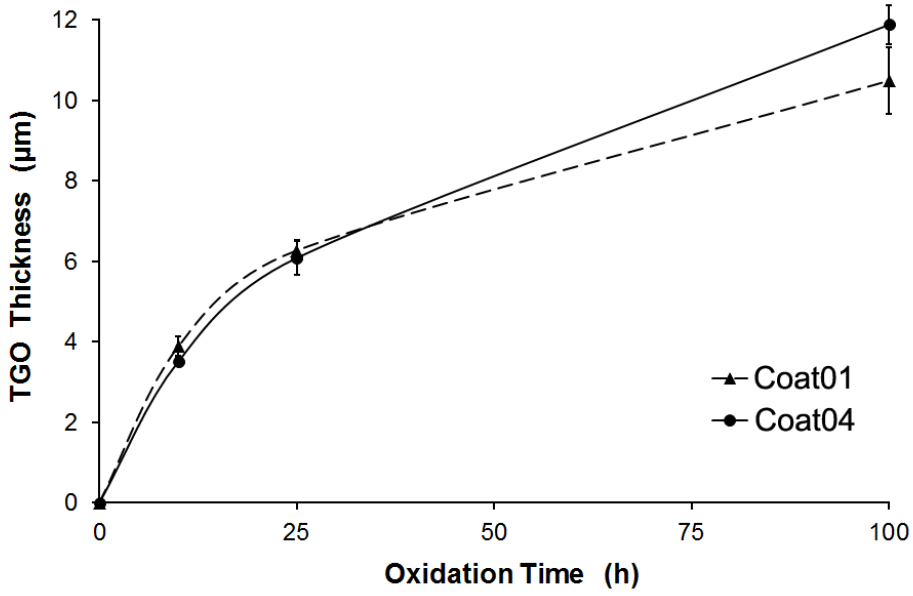

Figure 16. Evolution of the thickness of the thermally grown oxides (total oxide layer) in the Coat01 and Coat04 coatings tested as a function of oxidation time.

By using the weight gain and the oxide layer thickness, an experimental oxide density has been determined, such as the division of the normalized weight gain ΔW/A by the thickness

of the oxide layer, in Table 3. It can be seen that the Coat04 coating presents greater density in its layers of oxides at a time of 100 hours. Since the layers are porous, this density cannot be directly compared to the expected density. It is known that the density of rutile is 4.17 g/cm^3 and 3.97 g/cm^3 for alumina [1]. The obtained layers have half of the expected density, due to the presence of pores seen mainly in the more superficial layers, which would explain their growth.

Table 3. Experimental oxide density (mg/cm^3) for Coat01 and Coat04 coatings at different oxidation times

Coating	***Oxidation Time (h)***	***Experimental density of oxide layers (mg/cm^3)***
Coat01	10	1.305
	25	1.293
	100	1.452
Coat04	10	1.606
	25	1.578
	100	1.916

Underneath the oxide layer, an aluminum-depleted subsurface zone is observed, which is a possible indication of the initial formation of a layer containing α_2-Ti_3Al. It has been found that due to the low Al content in TiAl alloys, the oxidation process produces α_2-Ti_3Al at the oxide/metal interface. The existence of this phase can accelerate Ti penetration into the alumina and therefore decrease the oxidation resistance. This could explain the increase in oxidation rate after the initial state where a protective layer exists. However, the composition of this layer can be complex, and even the presence of a new cubic phase is mentioned [30]. By using transmission electron microscopy, several authors have been able to corroborate the presence of oxy-nitrures, which also affect resistance [26]. This layer of nitrures was not clearly observed in the laser coatings obtained in this investigation. Oxidation in air results in the formation of a nitrided layer under the oxide; this nitriding may be local or may allow a

system of Al_2O_3/TiN/Ti_2AlN/base metal layers. It is known that the presence of nitrogen increases the oxidation rate. The fragile layer of nitrides in the subsurface zone of the metal is detrimental if the part is subjected to mechanical stresses, because it facilitates the initiation of cracks. The nitriding of a crack front can increase its growth, according to *Kim et al.* [25] and *Becker et al.* [31]. In our case, the presence of cracks seen in the layers formed in some of the coatings is possibly explained by this theory (Figures 11 to 15).

The oxidation behavior of titanium aluminides based on γ-TiAl depends not only on the chemical composition of the material, but also on its microstructure. Some authors have found that the behavior depends mainly on the size and distribution of the phases, because for these alloys the amount of aluminum present is not enough to form stable Al_2O_3 [32]. By means of thermodynamic equilibrium calculations, the activity of aluminum and titanium in the α_2-Ti_3Al phase differs by several orders of magnitude from the γ-TiAl phase. Considering that alumina and rutile are oxidation products in equilibrium with Ti and Al, it was the case that TiO_2 is more stable than Al_2O_3 in α_2-Ti_3Al, and it is only in aluminum-rich phases like γ-TiAl that alumina can be stable, when formed during oxidation at elevated temperatures. In all cases, γ-TiAl is an alumina former, whereas α_2-Ti_3Al is a rutile former [32]. In this investigation, the Coat01 coating has a higher presence of γ-TiAl phase, so it is expected that a higher Al_2O_3 formation will improve the oxidation behavior compared to the Coat04 coating with its higher proportion of α_2-Ti_3Al, which favors the formation of TiO_2. Recent studies demonstrate the benefits of chromium and niobium in the corrosion resistance of TiAl laser metal deposition[33]. Therefore, it can be said that, when comparing the behavior of the substrate and the coating against oxidation, it has been found that, in terms of weight gain, the substrate generates a greater amount of oxide, and two groups of coating can be formed according to their microstructure. TiO_2/Al_2O_3/TiO_2+Al_2O_3/TiN multilayer scale are formed in the oxidized coatings and it was characterized by DRX, EDS on the surface and in cross section views.

Regarding the coatings, those in group 1 (Coat01 and Coat02) present better behavior against oxidation due to their microstructure composition, having a higher proportion of γ-TiAl compared to Coat03 and Coat04.

It is important to note that, in this study, the characterization of the oxide layers formed in the coatings obtained by laser metal deposition process was carried out, but it is also necessary to know, in depth, its evolution with oxidation time, in order to determine the resistance and adhesion of these oxide layers to the coating, which would guarantee their resistance to oxidation in the service condition.

4. Conclusions

The coatings can be divided into two groups according to the observed microstructure. Group 1 (formed by Coat01, with laser specific energy of 70 J/mm^2 and Coat02 with 80 J/mm^2), presents a duplex microstructure of γ-TiAl + α_2-Ti_3Al with zones of overlap between α_2-Ti_3Al cords. Group 2 (formed by Coat03, with laser specific energy of 90 J/mm^2, and Coat04 with 180 J/mm^2) presents grains of α_2-Ti_3Al and zones close to the re-melted area with a lamellar microstructure of γ-TiAl + α_2-Ti_3Al. The oxidation of the coatings generates layers of adherent oxides, from the surface to the coating, formed by TiO_2 + Al_2O_3 +TiO_2 + Al_2O_3 + TiN. On the other hand, the oxide layers generated on the substrate Ti6Al4V at 800 °C, have been detached after 5 hours of oxidation time. In general, the weight gain of the oxidized coatings indicates ten times more oxidation resistance for the Ti6Al4V substrate. For the substrate, this high weight gain is explained by the unsteadiness of the TiO_2 and Al_2O_3 layers that are formed, following a layer growth with increasing potential law.

The as-built microstructure is of great importance in Ti48Al2Cr2Nb laser coatings. For group 1 (Low specific energy), there is a lower weight gain than that presented by group 2 (High specific energy) due to the presence of more γ-TiAl phase, associated with greater amount of alumina, which decreases the growth rate of the oxide layers at early stage of oxidation.

For 100 hour of oxidation, there is a higher oxide layer thickness for Coat04 compared to Coat01, as well as higher oxide density. This indicates, in a preliminary way, that the coatings of group 1 have a better resistance to oxidation at 800 °C.

Laser metal deposition process can be used to generate TiAl coatings with good metallurgical bonding, high density, minimal dilution, and to improve the high-temperature oxidation behavior of components made with Ti6Al4V.

5. Acknowledgments

The authors would like to thank the Ministerio de Ciencia e Innovación of the Spanish Government for their financial support through research project MAT2011-28492-C03 and the Generalitat Valenciana through grant ACOMP/2014/151.

References

1. Leyens, C.; Peters, M. *Titanium and Titanium Alloys: Fundamentals and Applications*; Leyens, C., Peters, M., Eds.; John Wiley & Sons, 2003; ISBN 9783527305346.
2. Zhang, K. The Microstructure and properties of hipped powder Ti alloys, Ph.D Thesis. Birminghan University, Birmingham (UK), 2010.
3. Zambrano, J. C.; Cárcel, B.; Pereira, J. C.; Amigó, V. TiAl laser cladding coatings on Ti6Al4V: Tribological characterization | Recubrimientos laser cladding de TiAl sobre Ti6Al4V: Caracterización tribologica. *Rev. Latinoam. Metal. y Mater.* **2016**, *36*, 45–53.
4. De Oliveira, U.; Ocelík, V.; De Hosson, J. T. M. Analysis of coaxial laser cladding processing conditions. *Surf. Coatings Technol.* **2005**, *197*, 127–136, doi:10.1016/j.surfcoat.2004.06.029.
5. Tian, Y. S.; Chen, C. Z.; Li, S. T.; Huo, Q. H. Research progress on laser surface modification of titanium alloys. *Appl. Surf. Sci.* **2005**, *242*, 177–184, doi:https://doi.org/10.1016/j.apsusc.2004.08.011.
6. Yellup, J. M. Laser cladding using the powder blowing technique. *Surf. Coatings Technol.* **1995**, *71*, 121–128, doi:10.1016/0257-8972(94)01010-G.
7. Murr, L. E.; Gaytan, S. M.; Ceylan, A.; Martinez, E.; Martinez, J. L.; Hernandez, D. H.; Machado, B. I.; Ramirez, D. A.; Medina, F.; Collins, S.; Wicker, R. B. Characterization of titanium aluminide alloy components fabricated by additive manufacturing using electron beam melting. *Acta Mater.* **2010**, *58*, 1887–1894, doi:10.1016/j.actamat.2009.11.032.
8. Kothari, K.; Radhakrishnan, R.; Wereley, N. M. Advances in gamma titanium aluminides and their manufacturing techniques. *Prog. Aerosp. Sci.* **2012**, *55*, 1–16, doi:10.1016/j.paerosci.2012.04.001.
9. Brotzu, A.; Felli, F.; Pilone, D. Effect of alloying elements on the behaviour of TiAl-

based alloys. *Intermetallics* **2014**, *54*, 176–180, doi:10.1016/j.intermet.2014.06.007.

10. Brandao, P.; Infante, V.; Deus, A. M.; Pilone, D.; Brotzu, A.; Felli, F. Effect of surface modification on the stability of oxide scales formed on TiAl intermetallic alloys at high temperature. *Struct. Integr. Procedia Procedia Struct. Integr.* **2016**, *00*, 0–0, doi:10.1016/j.prostr.2016.06.287.
11. Abboud, J. H.; West, D. R. F. Microstructures of titanium-aluminides produced by laser surface alloying. *J. Mater. Sci.* **1992**, *27*, 4201–4207, doi:10.1007/BF01105127.
12. Appel, F.; Wagner, R. Microstructure and deformation of two-phase γ-titanium aluminides. *Mater. Sci. Eng. R* **1998**, *22*, 187–268, doi:10.1016/S0927-796X(97)00018-1.
13. Appel, F.; Oehring, M.; Wagner, R. Novel design concepts for gamma-base titanium aluminide alloys. *Intermetallics* **2000**, *8*, 1283–1312, doi:10.1016/S0966-9795(00)00036-4.
14. Dey, S. R.; Hazotte, A.; Bouzy, E. Crystallography and phase transformation mechanisms in TiAl-based alloys - A synthesis. *Intermetallics* **2009**, *17*, 1052–1064, doi:10.1016/j.intermet.2009.05.013.
15. Huang, Y.; Wang, Y.; Fan, H.; Shen, J. A TiAl based alloy with excellent mechanical performance prepared by gas atomization and spark plasma sintering. *Intermetallics* **2012**, *31*, 202–207, doi:10.1016/j.intermet.2012.07.006.
16. Maliutina, I. N.; Si-Mohand, H.; Piolet, R.; Missemer, F.; Popelyukh, A. I.; Belousova, N. S.; Bertrand, P. Laser Cladding of γ-TiAl Intermetallic Alloy on Titanium Alloy Substrates. *Metall. Mater. Trans. A* **2016**, *47*, 378–387, doi:10.1007/s11661-015-3205-9.
17. Sarkar, S.; Datta, S.; Das, S.; Basu, D. Oxidation protection of gamma-titanium aluminide using glass-ceramic coatings. *Surf. Coatings Technol.* **2009**, *203*, 1797–1805, doi:10.1016/j.surfcoat.2008.12.029.
18. Pilone, D.; Felli, F.; Brotzu, A. High temperature oxidation behaviour of TiAl-Cr-Nb-Mo alloys. *Intermetallics* **2013**, *43*, 131–137, doi:10.1016/j.intermet.2013.07.023.
19. Biamino, S.; Penna, A.; Ackelid, U.; Sabbadini, S.; Tassa, O.; Fino, P.; Pavese, M.; Gennaro, P.; Badini, C. Electron beam melting of Ti-48Al-2Cr-2Nb alloy: Microstructure and mechanical properties investigation. *Intermetallics* **2011**, *19*, 776–781, doi:10.1016/j.intermet.2010.11.017.
20. Lagos, M. A.; Agote, I. SPS synthesis and consolidation of TiAl alloys from elemental powders: Microstructure evolution. *Intermetallics* **2013**, *36*, 51–56, doi:10.1016/j.intermet.2013.01.006.
21. Loria, E. A. Gamma titanium aluminides as prospective structural materials. *Intermetallics* **2000**, *8*, 1339–1345, doi:10.1016/S0966-9795(00)00073-X.
22. Zhang, Y. Bin; Huang, B. Y.; Li, H. X. Influence of the Parameters on the Laser Deposited TiAl Layer. In *Emerging Focus on Advanced Materials*; Advanced Materials Research; Trans Tech Publications, 2011; Vol. 306, pp. 496–499.
23. Cárcel, B.; Serrano, A.; Zambrano, J.; Amigó, V.; Cárcel, A. C. Laser cladding of TiAl intermetallic alloy on Ti6Al4V. Process optimization and properties. In *Physics Procedia*; 2014; Vol. 56, pp. 284–293.
24. Jeng, S. C. Oxidation behavior and microstructural evolution of hot-dipped aluminum coating on Ti-6Al-4V alloy at 800 ^{o}C. *Surf. Coatings Technol.* **2013**, *235*, 867–874,

doi:10.1016/j.surfcoat.2013.09.023.

25. Kim, D. J.; Seo, D. Y.; Saari, H.; Sawatzky, T.; Kim, Y. W. Isothermal oxidation behavior of powder metallurgy beta gamma TiAl-2Nb-2Mo alloy. *Intermetallics* **2011**, *19*, 1509–1516, doi:10.1016/j.intermet.2011.05.027.

26. Haanappel, V. A. C.; Hofman, R.; Sunderkötter, J. D.; Glatz, W.; Clemens, H.; Stroosnijder, M. F. The influence of microstructure on the isothermal and cyclic-oxidation behavior of Ti-48Al-2Cr at 800 ^{o}C. *Oxid. Met.* **1997**, *48*, 263–287, doi:10.1007/BF01670503.

27. Haanappel, V. A. .; Clemens, H.; Stroosnijder, M. . The high temperature oxidation behaviour of high and low alloyed TiAl-based intermetallics. *Intermetallics* **2002**, *10*, 293–305, doi:10.1016/S0966-9795(01)00137-6.

28. Schmitz-Niederau, M.; Schutze, M. The Oxidation Behavior of Several Ti-Al Alloys at 900 ^{o}C in Air. *Oxid. Met.* **1999**, *52*, 225–240, doi:10.1023/A:1018839511102.

29. Varlese, F. A.; Tului, M.; Sabbadini, S.; Pellissero, F.; Sebastiani, M.; Bemporad, E. Optimized coating procedure for the protection of TiAl intermetallic alloy against high temperature oxidation. *Intermetallics* **2013**, *37*, 76–82, doi:10.1016/j.intermet.2013.02.001.

30. Yang, M.-R.; Wu, S. K. Oxidation Resistance Improvement of TiAl Intermetallics Using Surface Modification. *Bull. Coll. Eng.* **2003**, 3–19.

31. Becker, S.; Rahmel, A.; Schorr, M.; Schütze, M. Mechanism of isothermal oxidation of the intel-metallic TiAl and of TiAl alloys. *Oxid. Met.* **1992**, *38*, 425–464, doi:10.1007/BF00665663.

32. Gil, A.; Hoven, H.; Wallura, E.; Quadakkers, W. J. The effect of microstructure on the oxidation behaviour of TiAl-based intermetallics. *Corros. Sci.* **1993**, *34*, 615–630, doi:10.1016/0010-938X(93)90276-M.

33. Maliutina, I. N.; Si-Mohand, H.; Sijobert, J.; Bertrand, P.; Lazurenko, D. V.; Bataev, I. A. Structure and oxidation behavior of γ-TiAl coating produced by laser cladding on titanium alloy. *Surf. Coatings Technol.* **2017**, *319*, 136–144, doi:10.1016/j.surfcoat.2017.04.008.

Figure1
Click here to download high resolution image

Figure2

Click here to download high resolution image

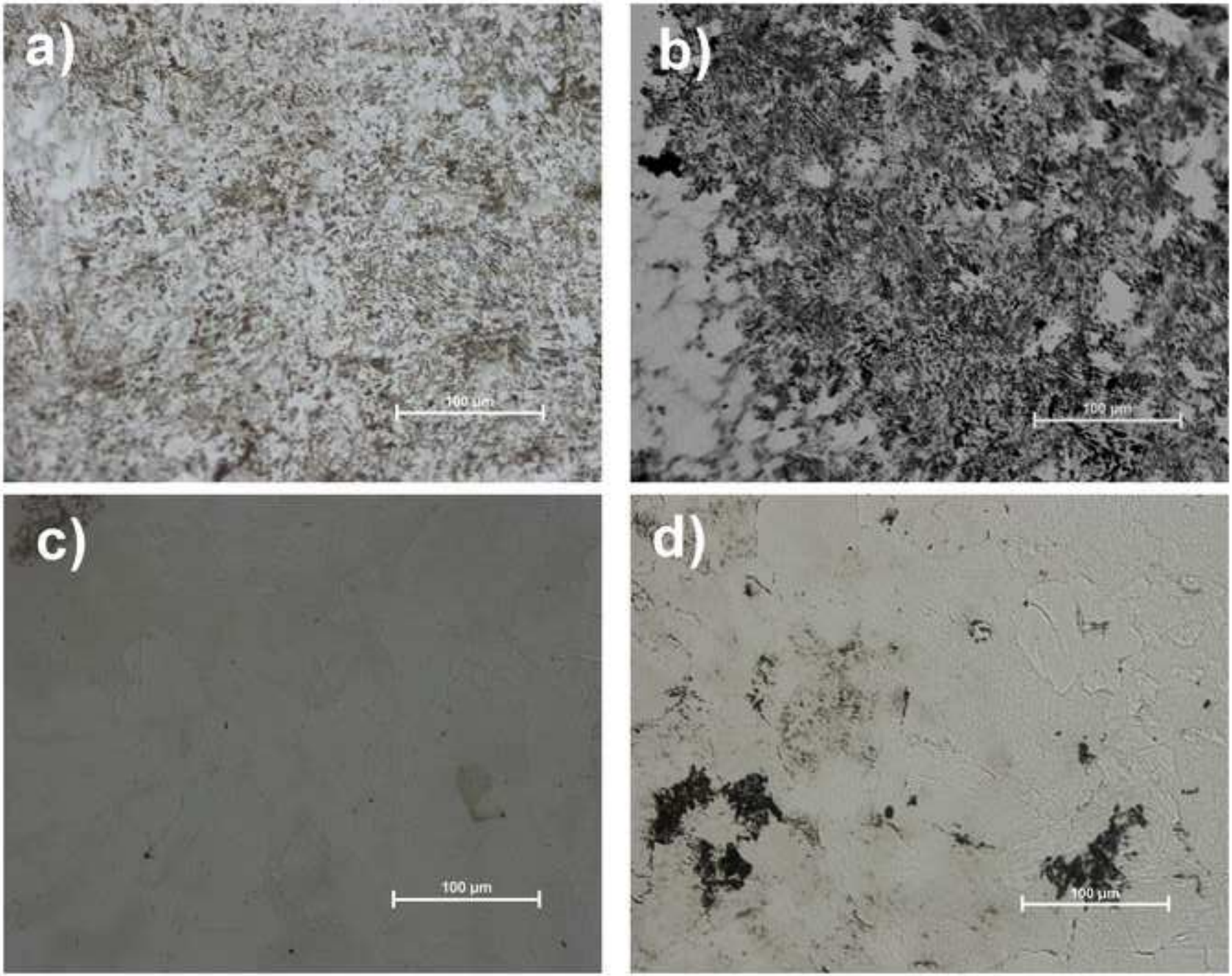

Figure3

Click here to download high resolution image

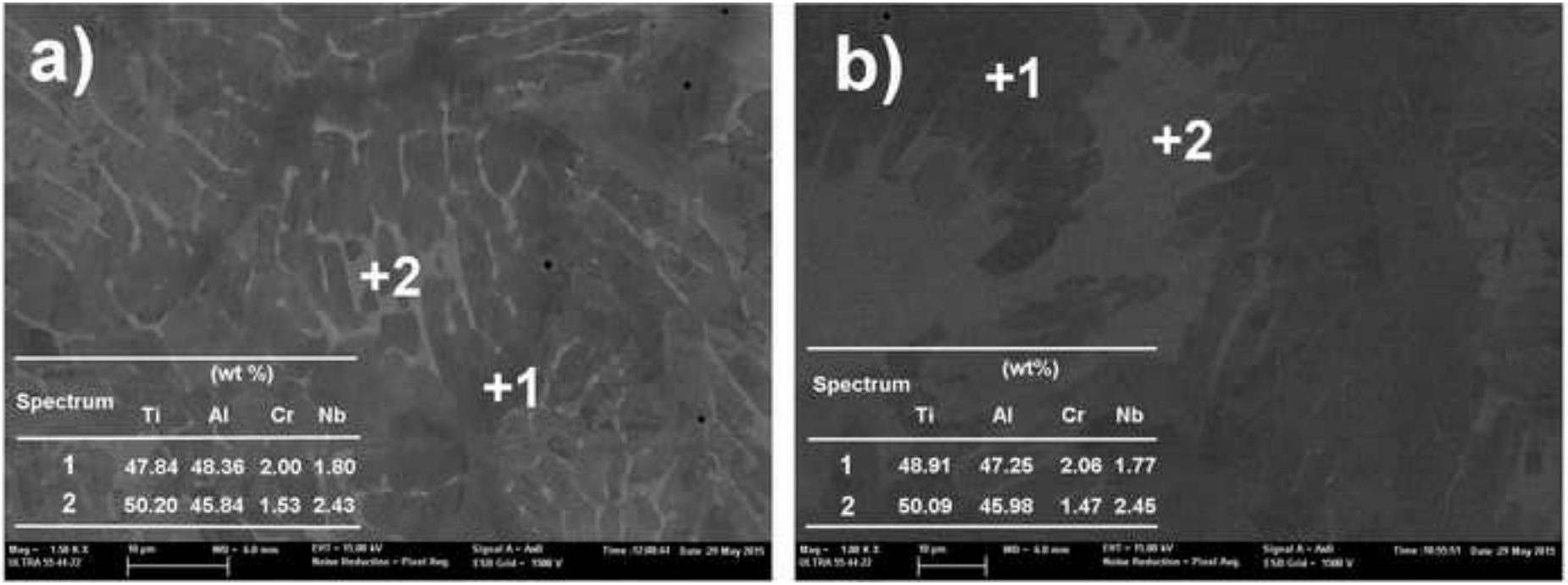

Figure4

Click here to download high resolution image

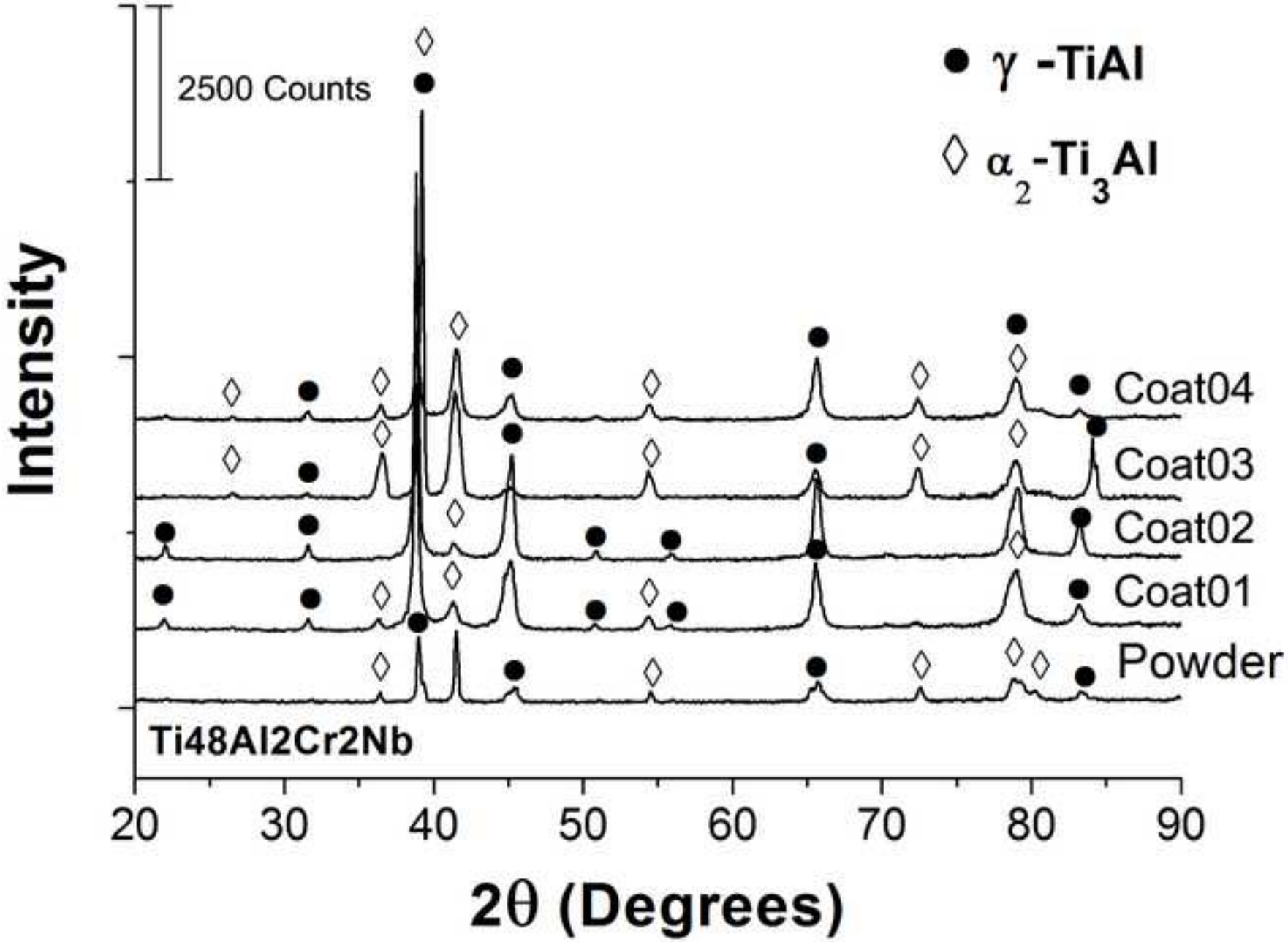

Figure5
Click here to download high resolution image

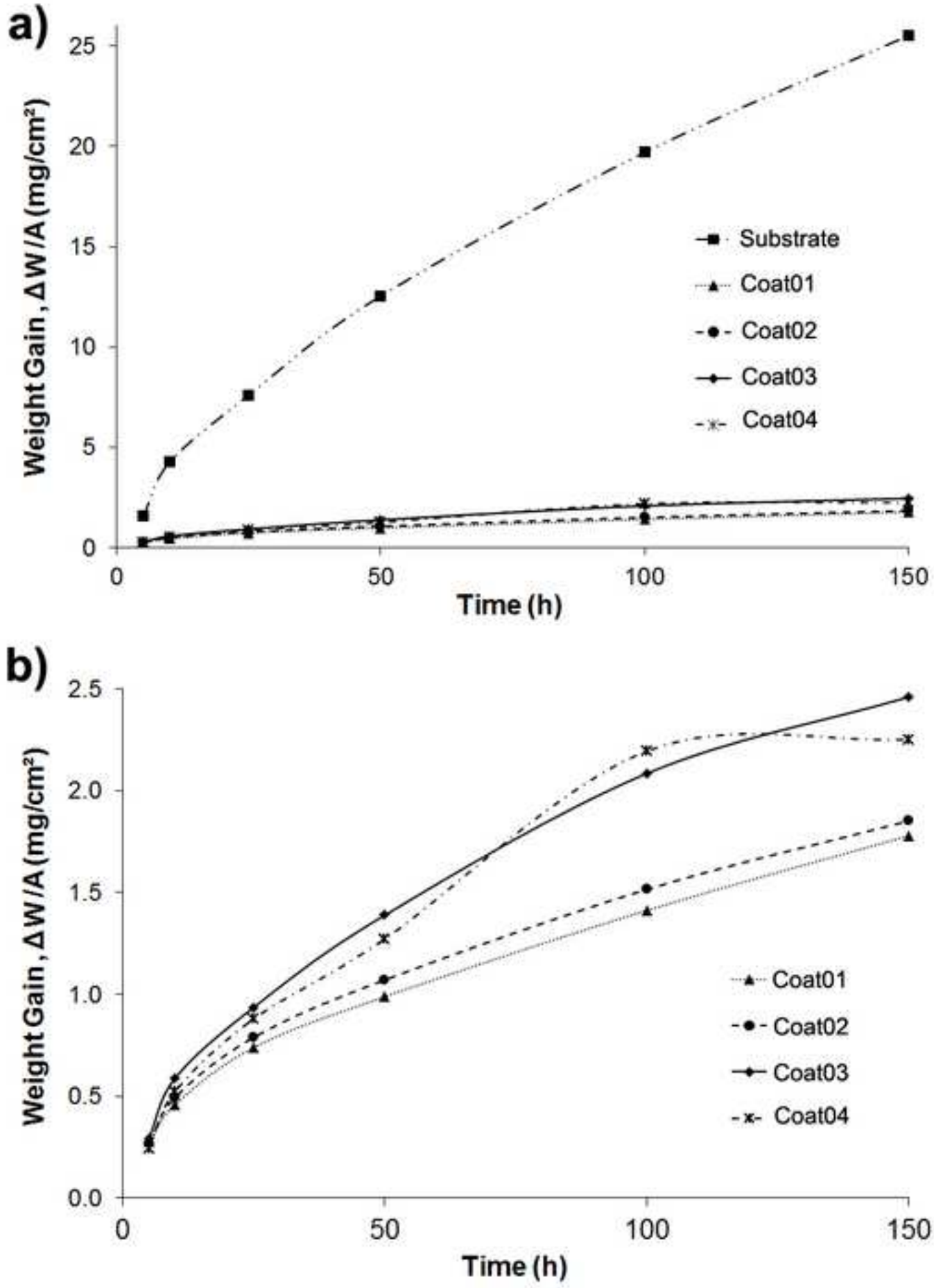

Figure6

Click here to download high resolution image

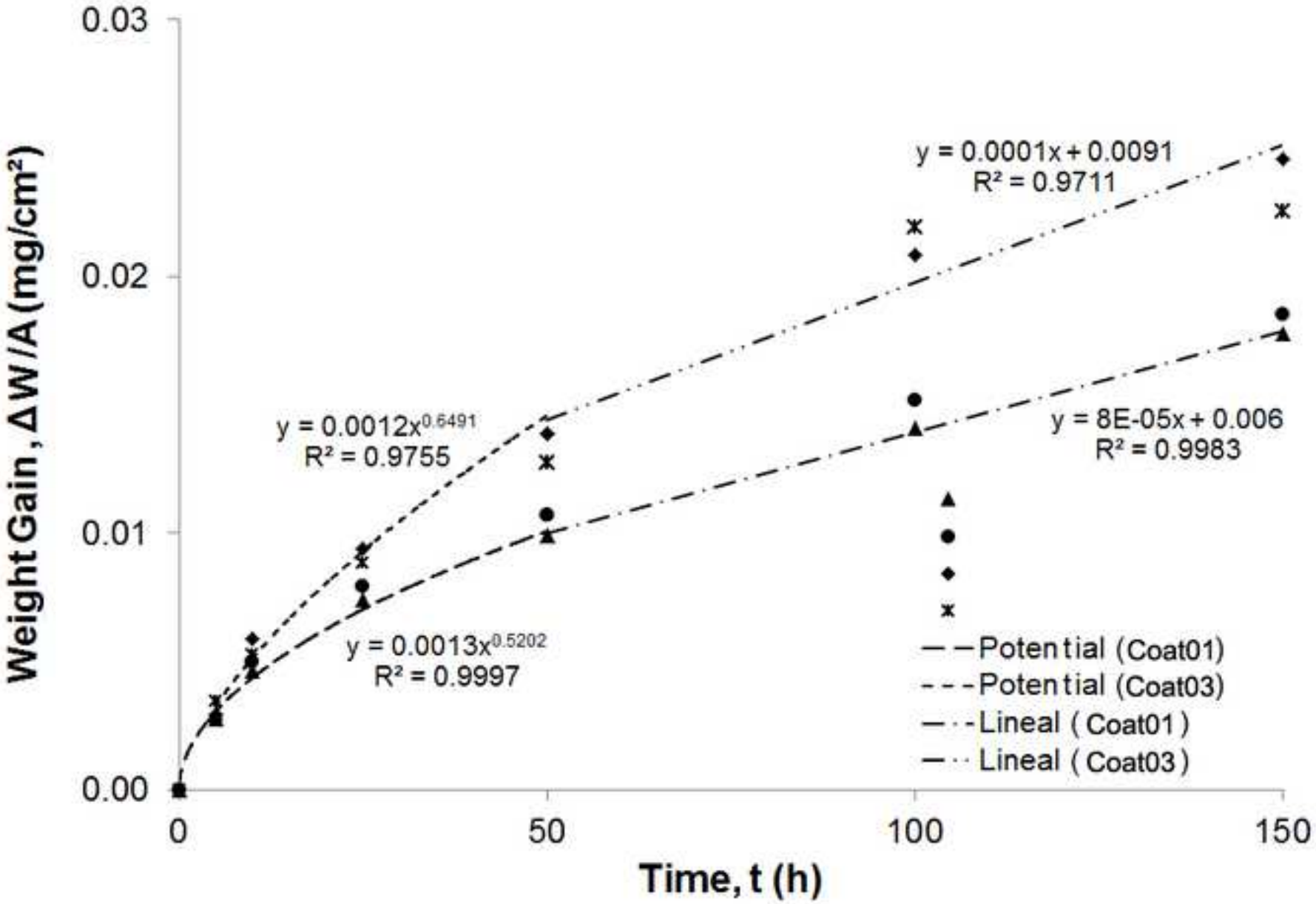

Figure7

Click here to download high resolution image

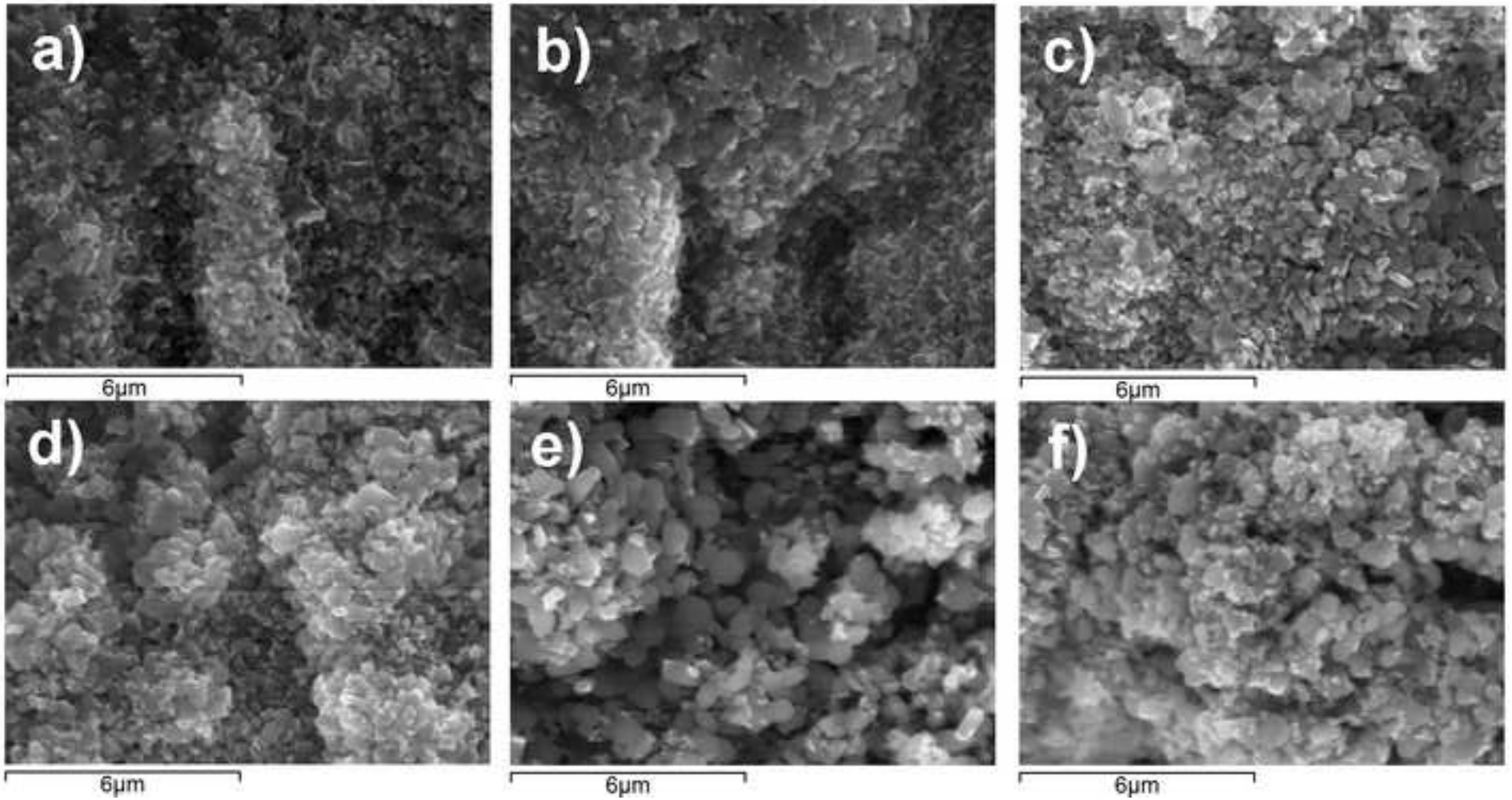

Figure8

Click here to download high resolution image

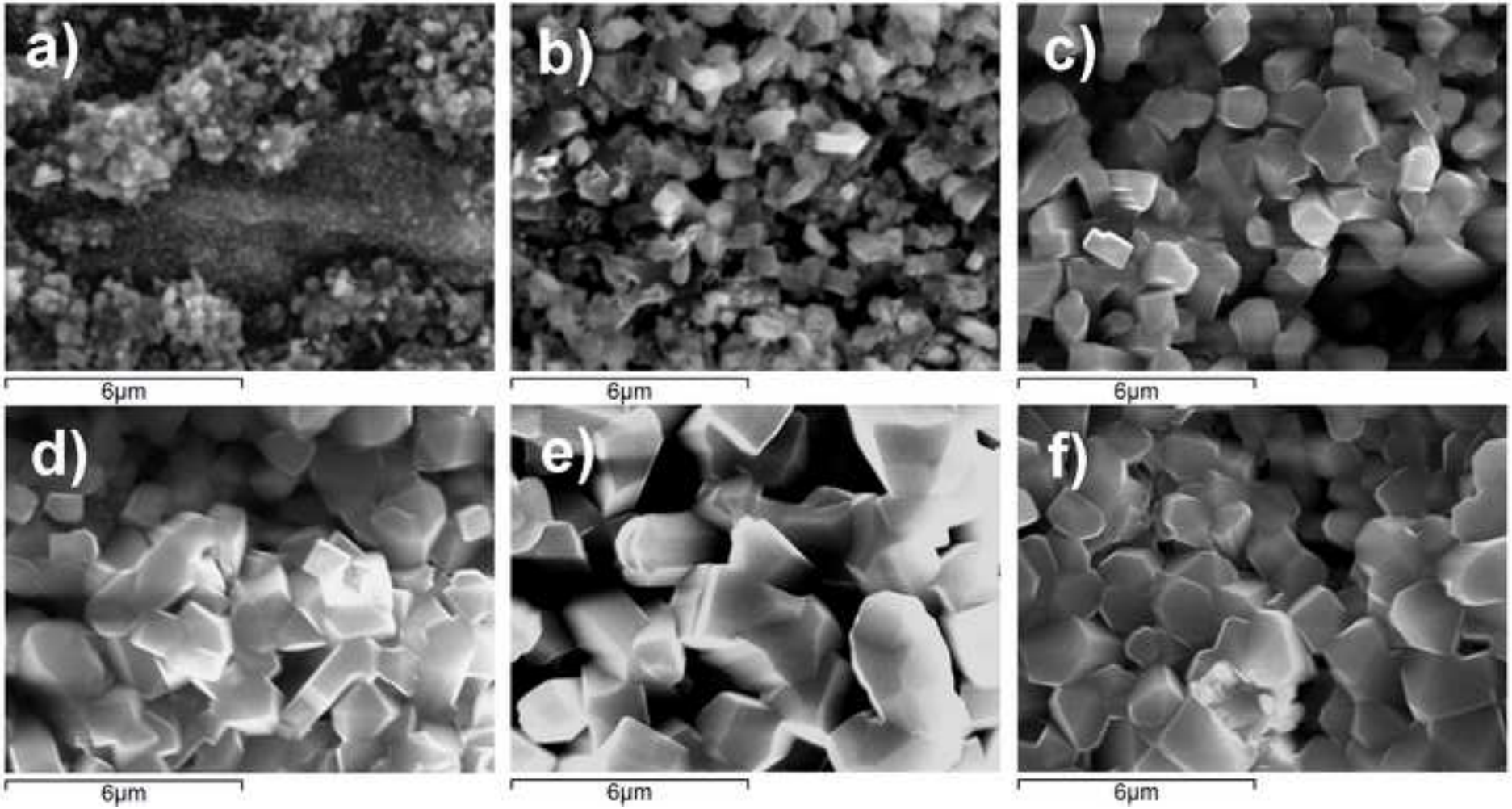

Figure9

Click here to download high resolution image

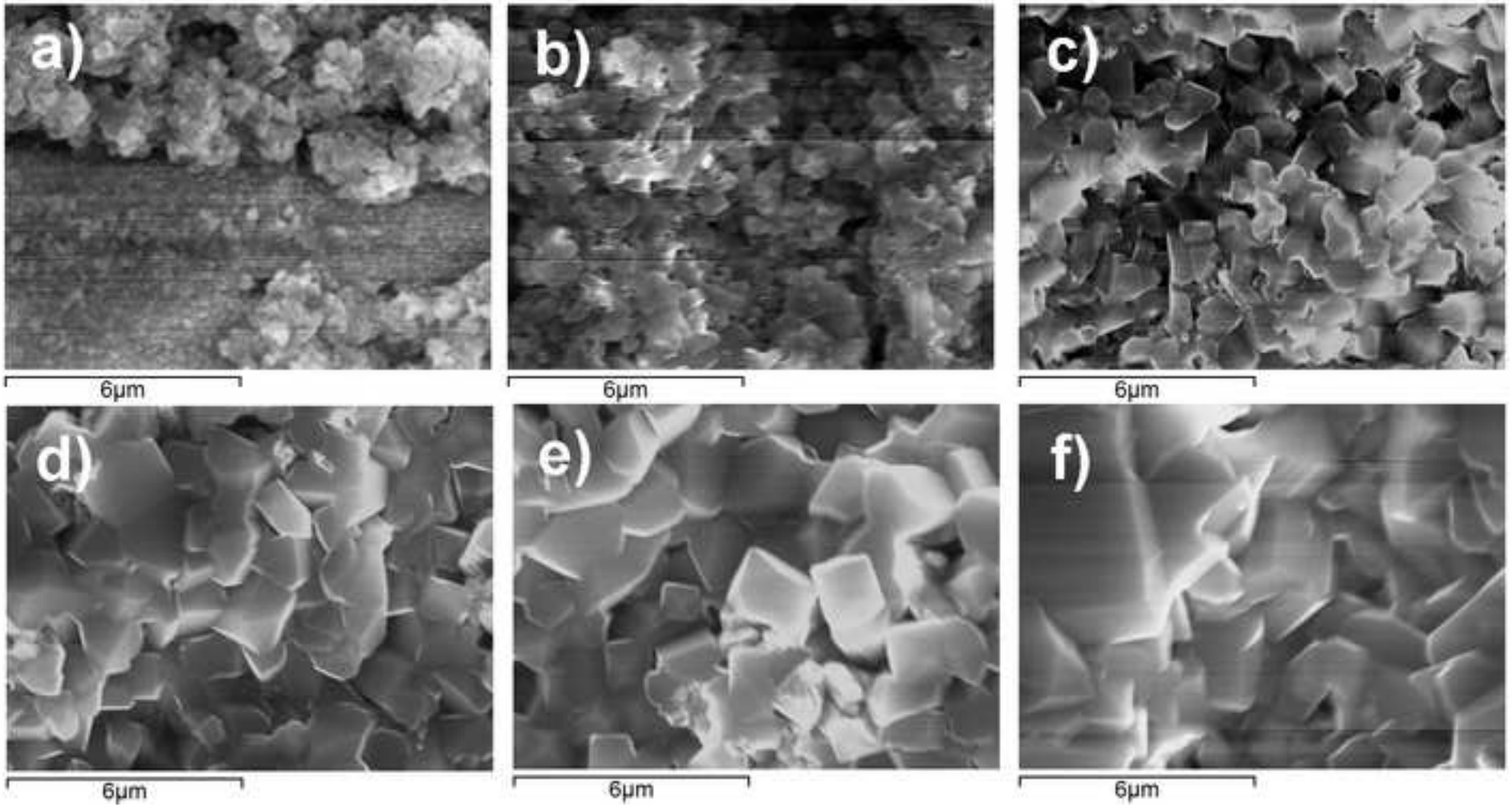

Figure10

Click here to download high resolution image

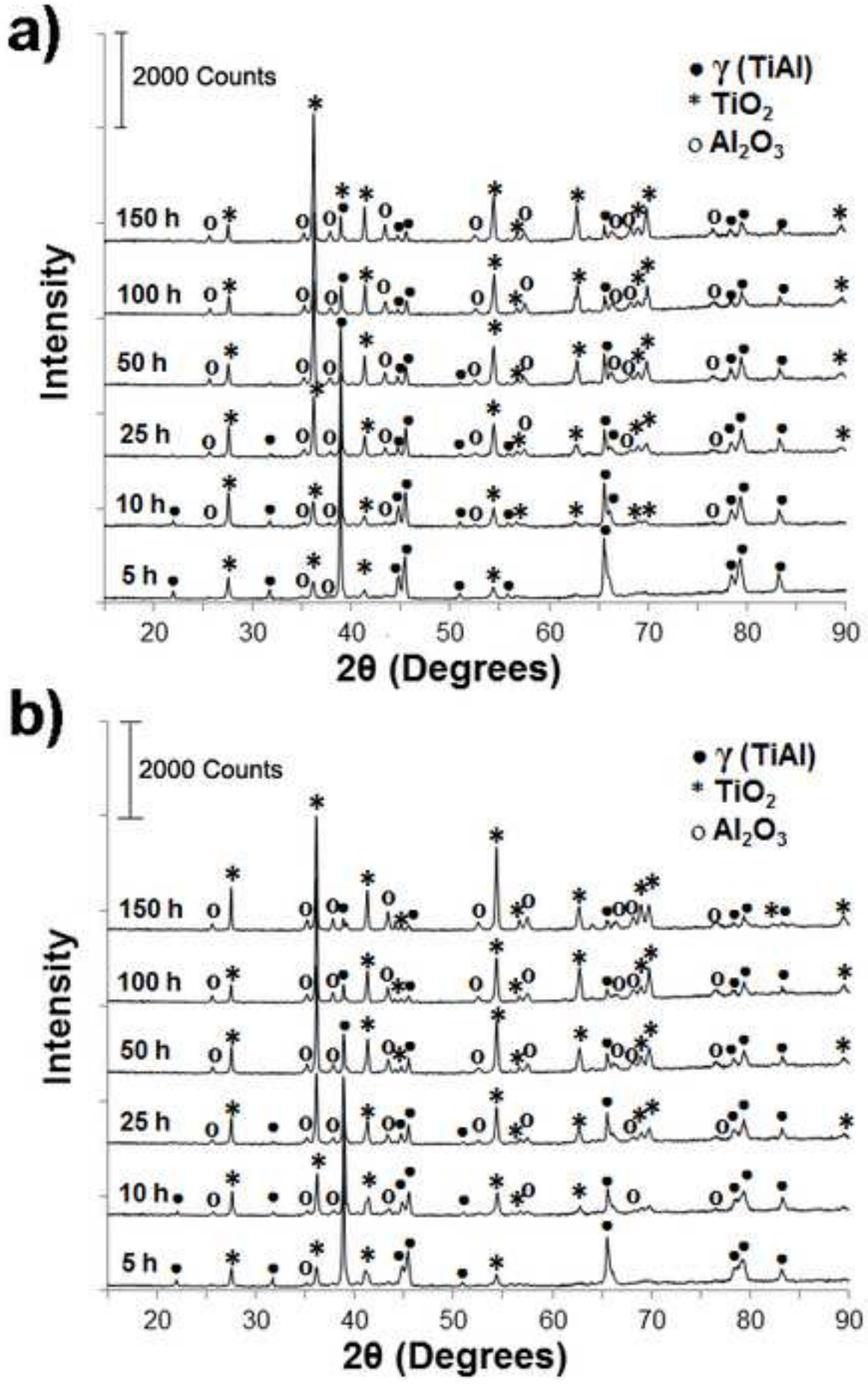

Figure11

Click here to download high resolution image

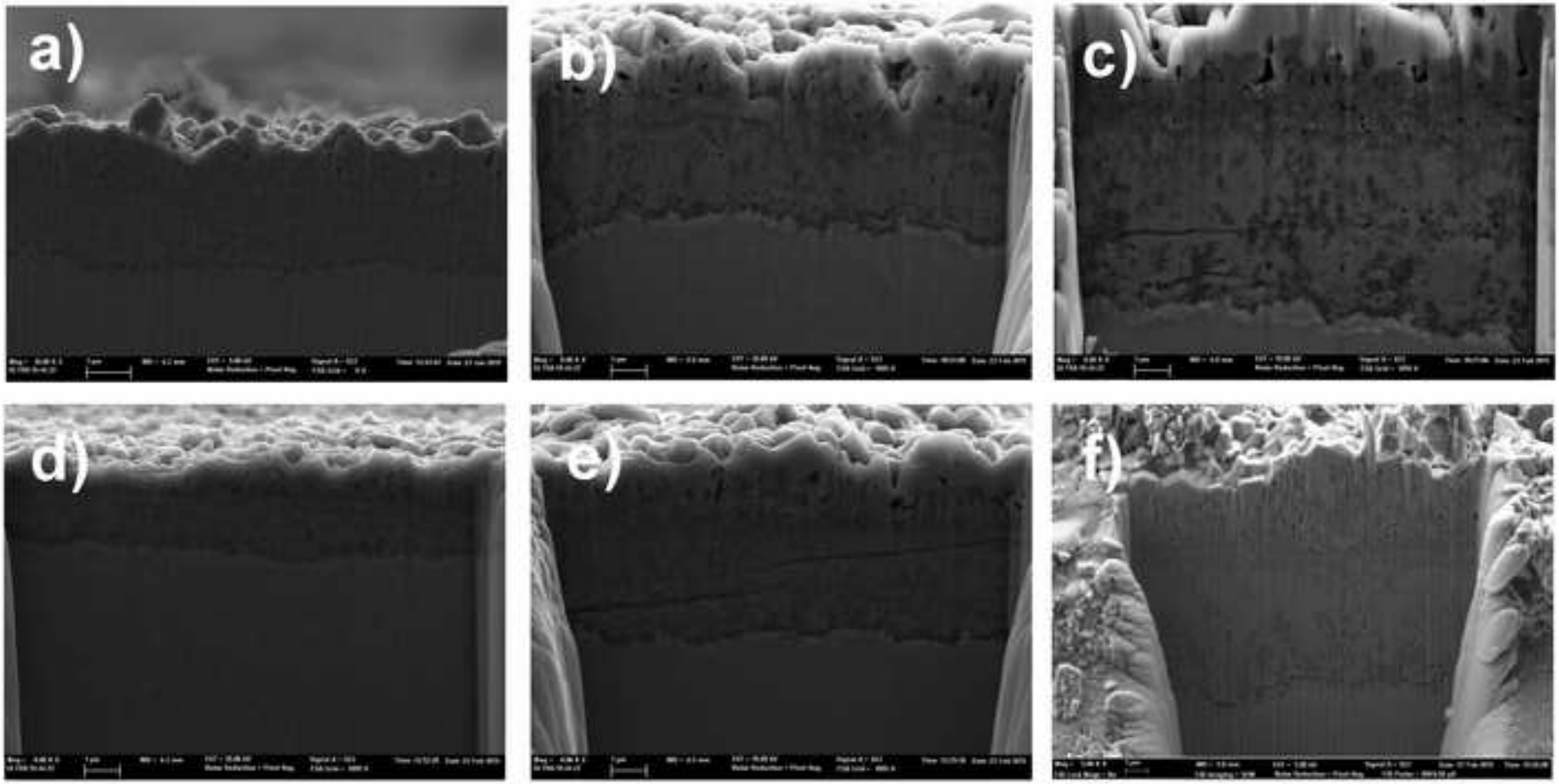

Figure12

Click here to download high resolution image

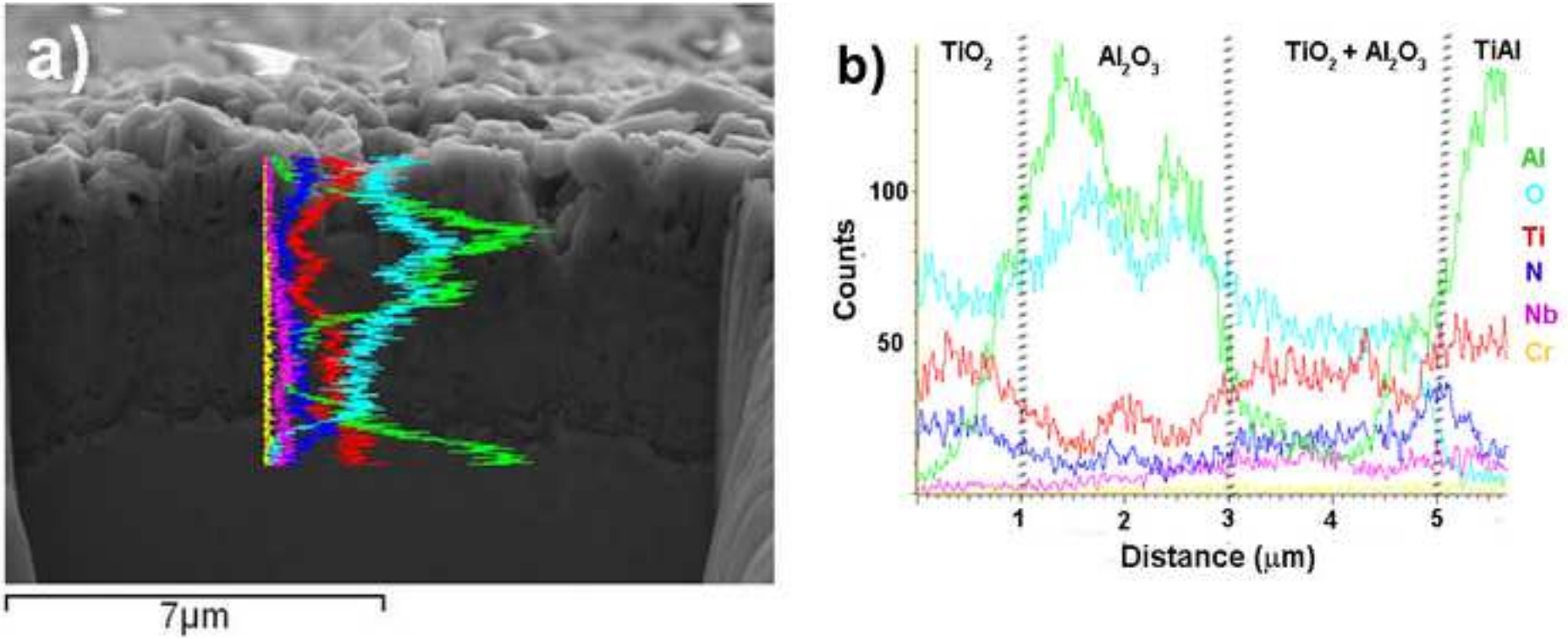

Figure13

Click here to download high resolution image

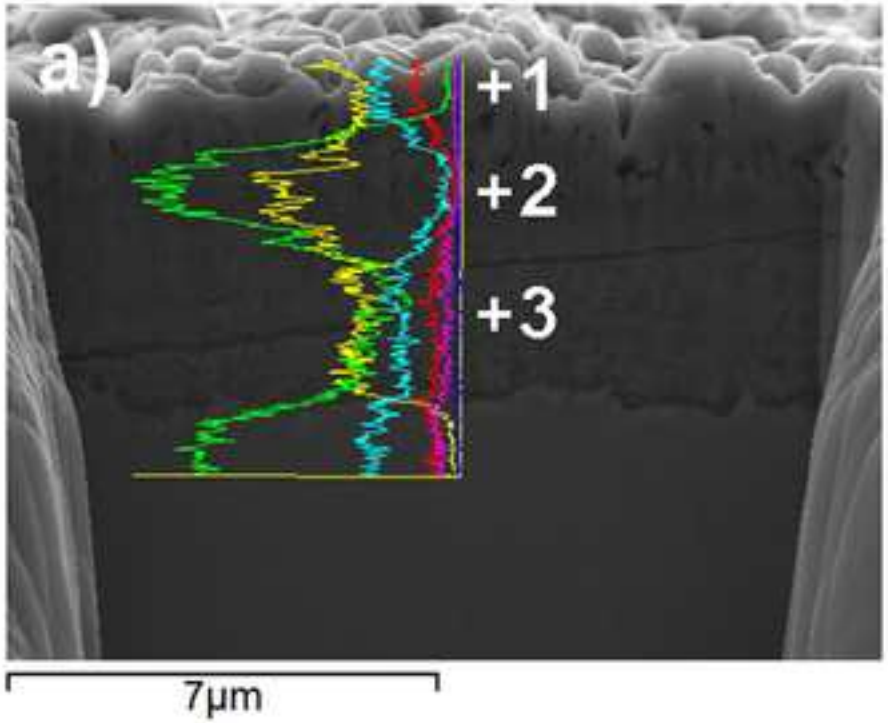

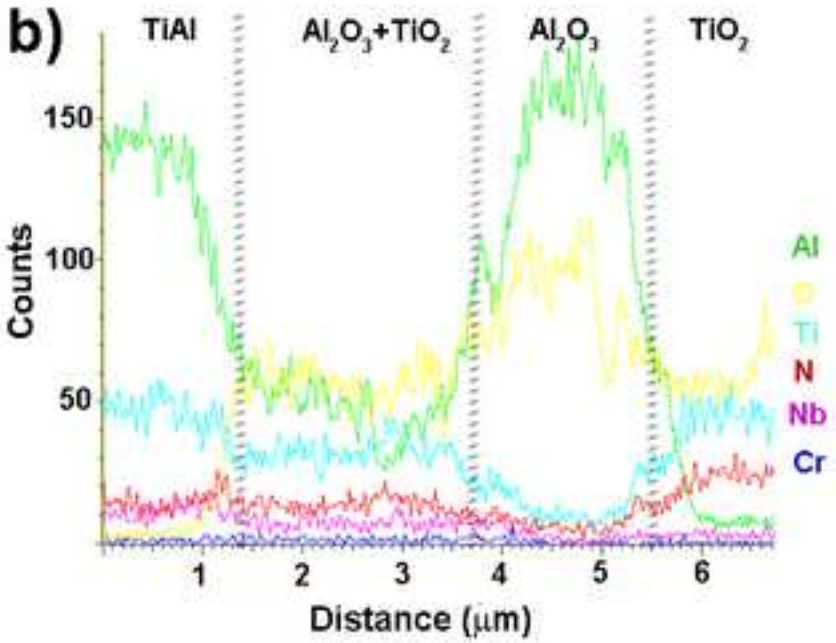

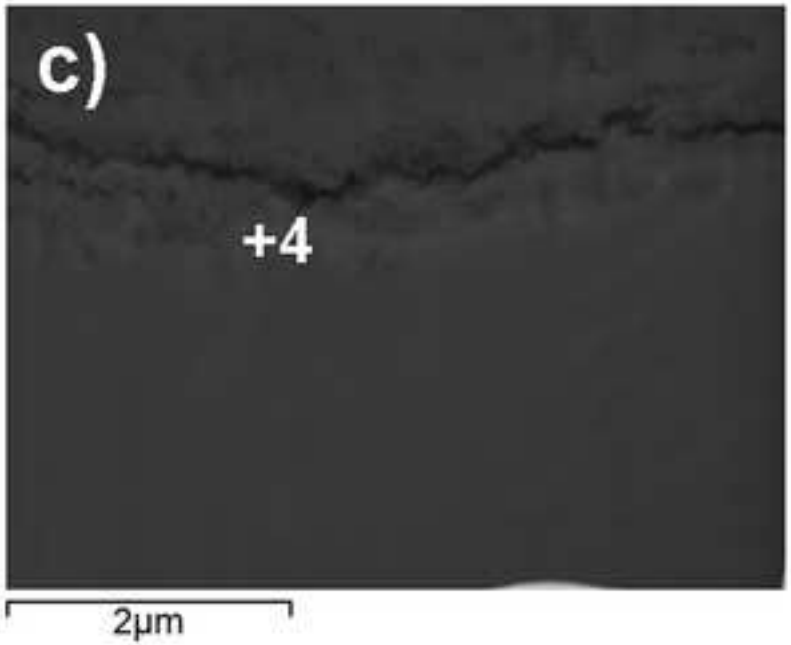

d)

Espectrum	Wt %					
	O	Al	Ti	Cr	Nb	N
1	49.25	0.82	49.93	0	0	0
2	49.53	35.54	9.18	4.98	0.77	0
3	42.68	8.69	35.98	8.23	4.42	0
4	22.82	19.94	39.69	7.61	5.98	3.96

Figure14

Click here to download high resolution image

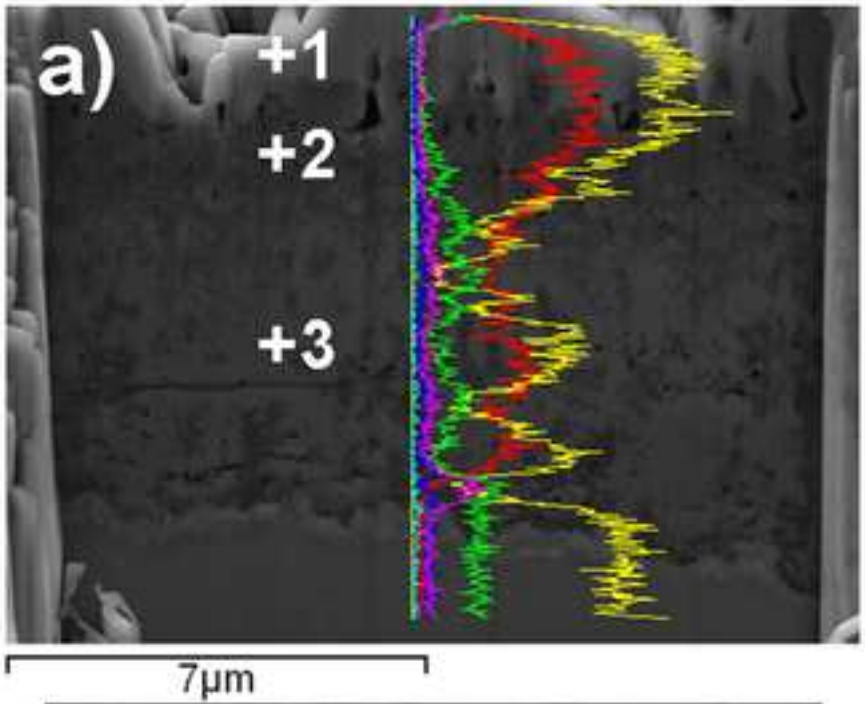

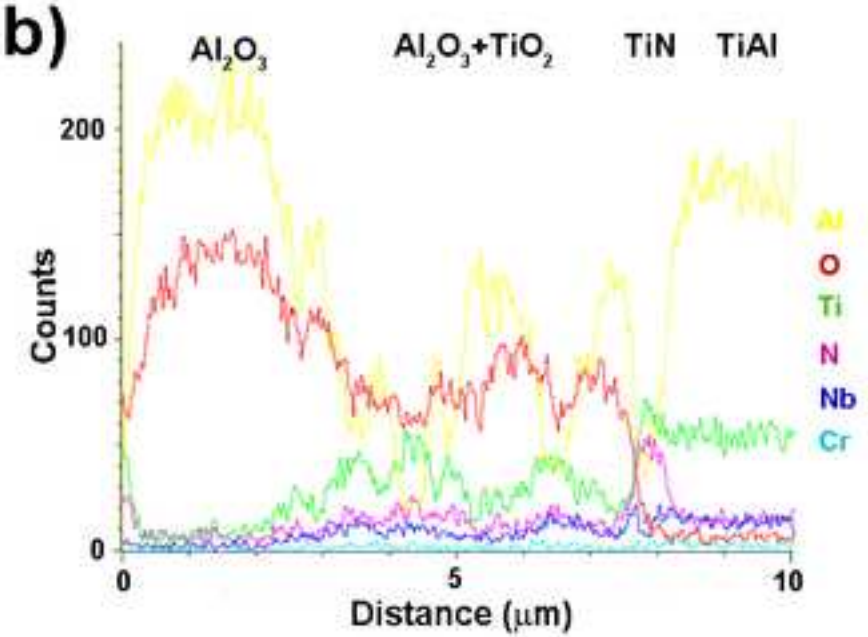

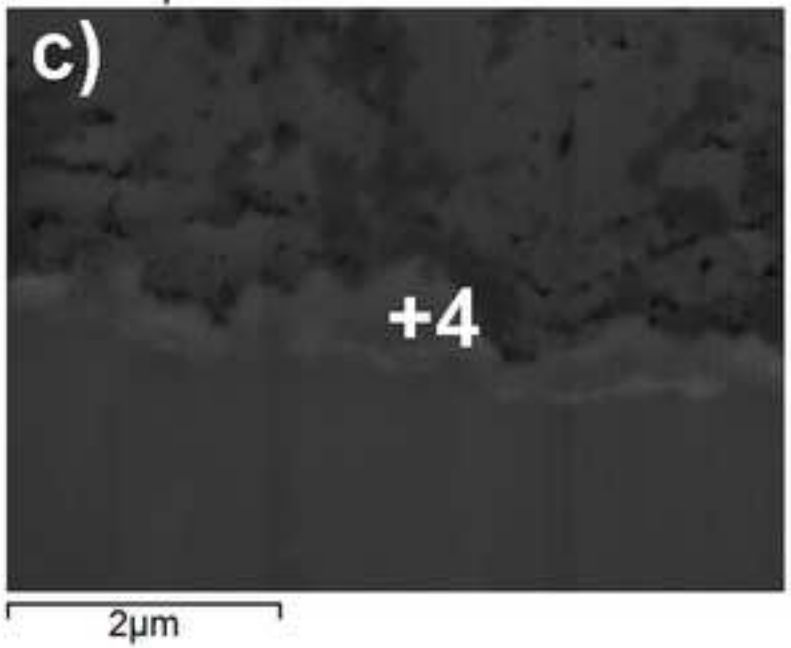

d)

Espectrum	Wt %					
	O	Al	Ti	Cr	Nb	N
1	47.59	1.32	51.08	0	0	0
2	52.42	35.01	10.63	1.83	0.11	0
3	39.56	3.35	42.64	8.83	5.62	0
4	7.18	5.97	59.57	9.03	3.84	14.42

Figure15

Click here to download high resolution image

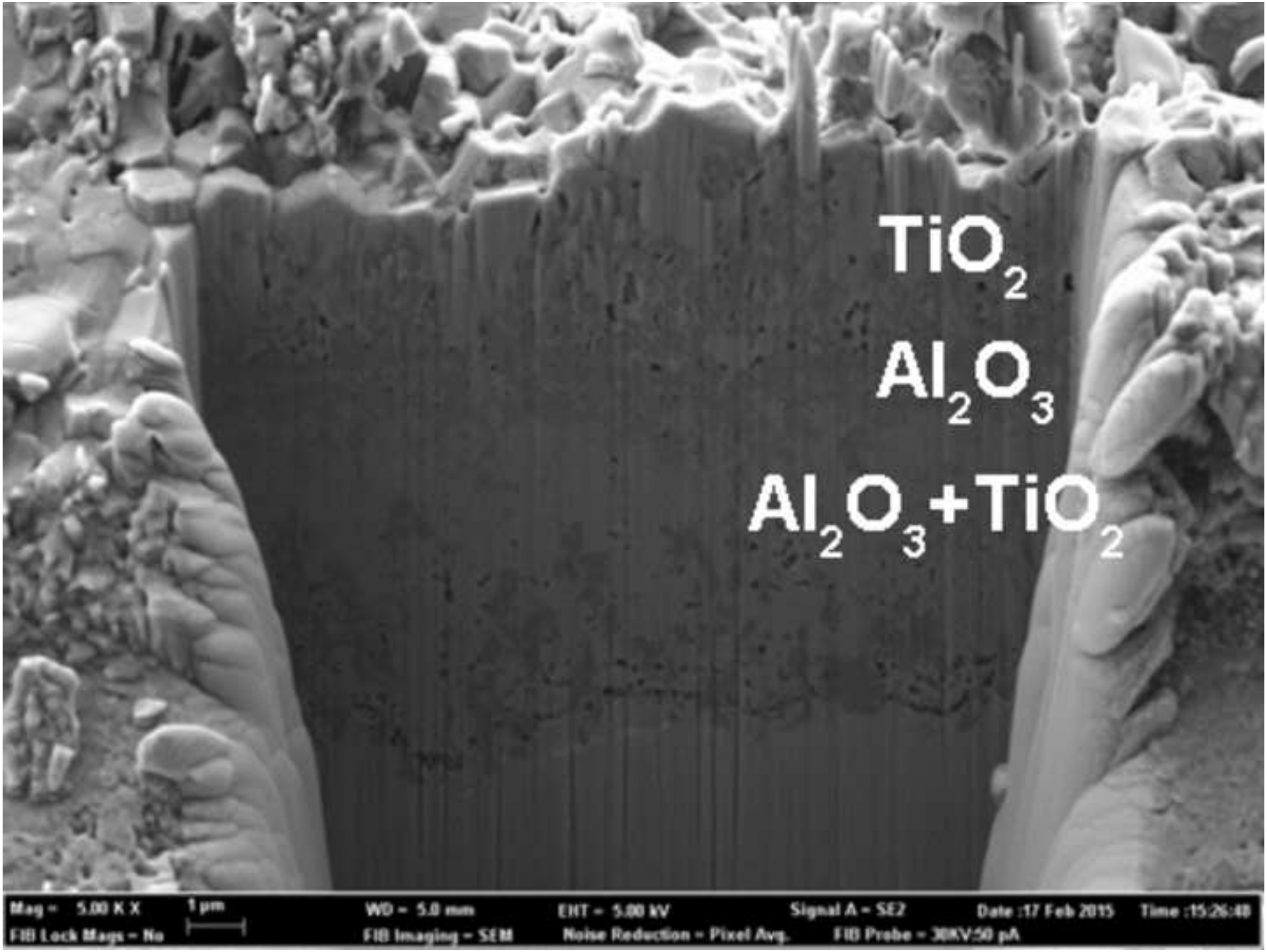

Figure16

Click here to download high resolution image

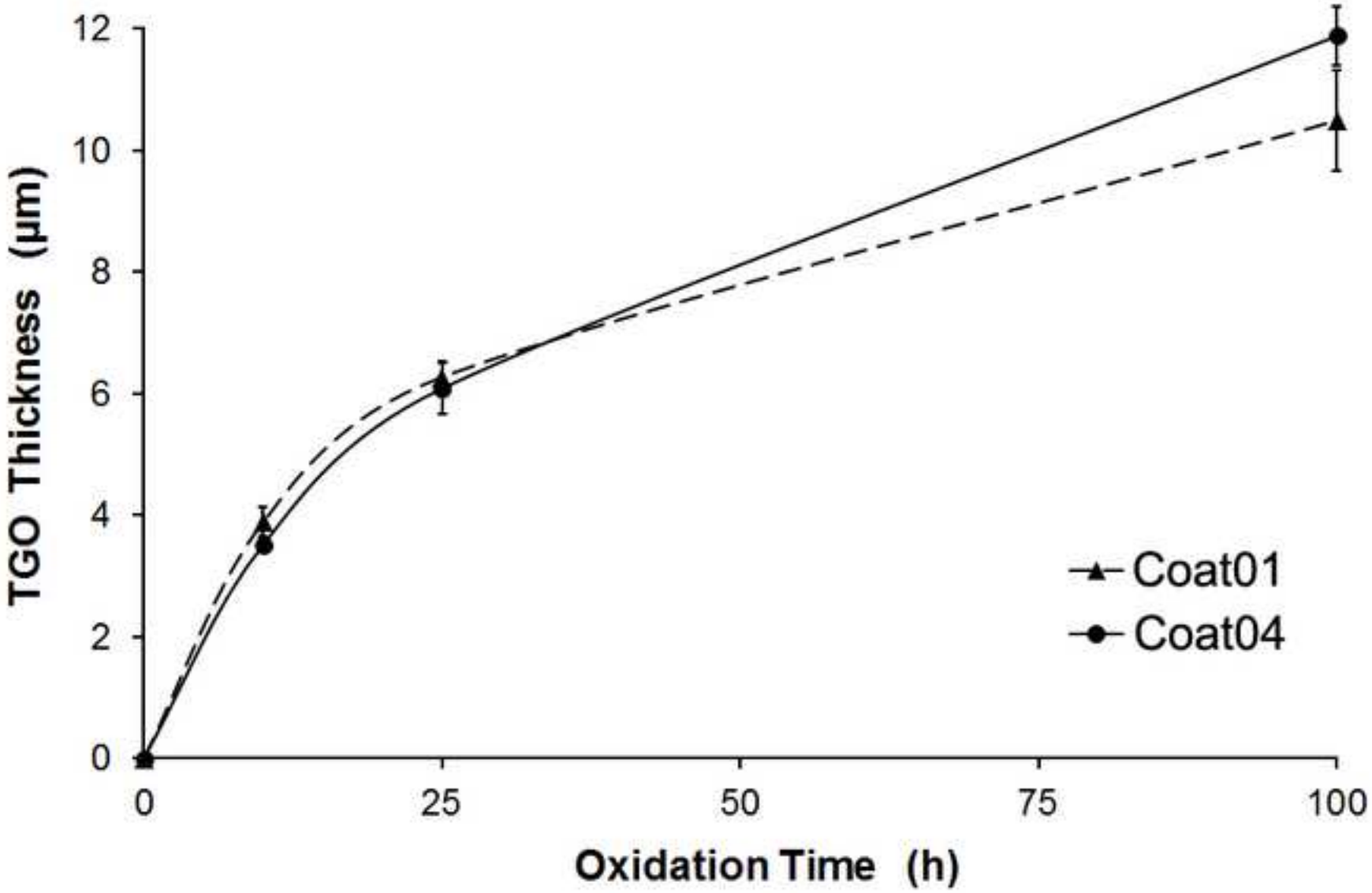

Recommended reviewers:

Eli Saul Puchi-Cabrera, Dr
Specialist in characterization of metallic coatings
Université Lille Nord de France, UVHC, LAMIH UMR CNRS 8201, Valenciennes F-59313, France
eli.puchicabrera@univ-valenciennes.fr
eli.puchi@univ-lille1.fr

Andres Gasser, PhD
Specialist in laser cladding and laser metal deposition for additive manufacturing
Fraunhofer Institute for Laser Technology ILT, Steinbachstr. 15
52074 Aachen, Germany
Phone +49 241 8906-209
Fax +49 241 8906-121
andres.gasser@ilt.fraunhofer.de

Cleiton Carvalho Silva
Specialist in Ni-based coatings and Laser Processing Materials
Universidade Federal do Ceará (UFC),
Engenharia Metalúrgica e de Materiais, Fortaleza, Brazil
cleiton@metalmat.ufc.br
Author ID: 56314981400
http://orcid.org/0000-0001-6827-8939

Mariana Staia
Specialist in metallic coatings and tribology
mhstaia@gmail.com
Arts et Métiers ParisTech, MSMP, Centre de Lille, 8, Boulevard Louis XIV, 59000 Lille Cedex, France

João Batista Fogagnolo, Dr
Specialist in Laser Processing Materials
fogagnolo@fem.unicamp.br
Scopus Author ID: Author ID: 6602138253
UNICAMP – University of Campinas, School of Mechanical Engineering, Rua Mendeleiev 200, 13083-860 Campinas, SP, Brazil
Tel.: +55 19 35213300; fax: +55 19 32893722.

Graphical Abstract

Click here to download high resolution image